NextScour Case Study: The Lafayette Avenue Bridge Over the Saginaw River in Bay City, Michigan

PUBLICATION NO. FHWA-HRT-23-014

JANUARY 2023

U.S. Department of Transportation
Federal Highway Administration

Research, Development, and Technology
Turner-Fairbank Highway Research Center
6300 Georgetown Pike
McLean, VA 22101-2296

FOREWORD

The Federal Highway Administration (FHWA) is developing the NextScour Research Initiative with the goal of improving scour analysis and providing more accurate scour depth estimates for bridge foundation design. This initiative is an interdisciplinary effort between hydraulics and geotechnical engineers to address the existing knowledge gaps surrounding traditional methods of scour analysis. In 2020, FHWA established a Transportation Pooled Fund study to collaborate with State departments of transportation on future bridge projects at sites with layers of cohesive soils that could potentially provide resistance to hydraulic loads. This report documents one of the case studies, Lafayette Avenue Bridge in Michigan, and provides an example of how the NextScour approach can assist practitioners as they calculate scour depths and conduct bridge foundation design.

Mark E. Swanlund
Acting Director, Office of Infrastructure
Research and Development

.

TECHNICAL REPORT DOCUMENTATION PAGE

1. Report No. FHWA-HRT-23-014	2. Government Accession No.	3. Recipient's Catalog No.
4. Title and Subtitle NextScour Case Study: The Lafayette Avenue Bridge Over the Saginaw River in Bay City, Michigan		5. Report Date January 2023 6. Performing Organization Code:
7. Author(s) with ORCID numbers. Haoyin Shan (0000-0002-6358-5347), James Pagenkopf (0000-0001-5392-8628), Chen Li (0000-0001-6915-9368), Nasi Zhang (0000-0002-1175-6909), Daniel Pastrich (0000-0003-1417-1989), Otto Wiblishauser (0000-0002-1257-8163), Chao Huang (0000-0002-6034-8637), and Kornel Kerenyi (0000-0002-7363-2223).		8. Performing Organization Report No.
9. Performing Organization Name and Address Genex Systems, LLC 11848 Rock Landing Drive, Suite 303 Newport News, VA 23606		10. Work Unit No. 11. Contract or Grant No. 693JJ320F000313
12. Sponsoring Agency Name and Address Office of Research, Development, and Technology Federal Highway Administration 6300 Georgetown Pike McLean, VA 22101-2296		13. Type of Report and Period Covered Research Report; October 2020–August 2022 14. Sponsoring Agency Code HRDI-40

15. Supplementary Notes

The Contracting Officer's Representative was Kornel Kerenyi (HRDI-40, 0000-0002-7363-2223). The authors thank Dr. Zhaoding Xie and Ms. Xinya Liu for their technical assistance with two- and three-dimensional computational fluid dynamics modeling, and Mr. Nandor Nagy for his assistance on preparing figures in this paper.

16. Abstract

The Michigan Department of Transportation (MDOT) plans to replace the Lafayette Avenue Bridge over the Saginaw River in Bay City, MI. Hydraulic scour analysis of the planned bridge replacement resulted in deep scour depths, which MDOT believed were excessive due to a subsurface layer of cohesive soil that existed across the bridge site. MDOT reached out to the Federal Highway Administration (FHWA) to inquire if FHWA's NextScour Research Initiative could potentially reduce the scour design depths. Additionally, both the existing bridge and proposed bridge replacement featured large bascule piers, and MDOT asked if FHWA could conduct physical modeling of the piers in their flume to study scour formations around the piers.

Through a Transportation Pooled Fund study, TPF-5(461), FHWA was able to perform five tasks for MDOT that are summarized in this report (FHWA 2020). Task 1: Perform hydraulic modeling of the site to obtain flow velocities and bed shear stresses. Task 2: Perform soil erosion testing on the cohesive soil to determine the clay's critical shear stress. Task 3: Develop decay functions to establish the relation between hydraulic loads and depth. Task 4: Conduct computational fluid dynamics scour modeling in sand and clay soils. Task 5: Conduct a probabilistic scour analysis to quantify the risk levels for the various scour analysis methods. This research study showed that the cohesive layer of clay at the site could potentially stop the scour at this bridge site, and the NextScour methodology is a developing tool to improve accuracy for bridge foundation design.

17. Key Words NextScour, scour design, hydraulic modeling, soil erosion testing, computational fluid dynamics, and probabilistic analysis	18. Distribution Statement No restrictions. This document is available to the public through the National Technical Information Service, Springfield, VA 22161. http://www.ntis.gov		
19. Security Classif. (of this report) Unclassified	20. Security Classif. (of this page) Unclassified	21. No. of Pages 57	22. Price N/A

Form DOT F 1700.7 (8-72) Reproduction of completed page authorized

SI* (MODERN METRIC) CONVERSION FACTORS

APPROXIMATE CONVERSIONS TO SI UNITS

Symbol	When You Know	Multiply By	To Find	Symbol
		LENGTH		
in	inches	25.4	millimeters	mm
ft	feet	0.305	meters	m
yd	yards	0.914	meters	m
mi	miles	1.61	kilometers	km
		AREA		
in^2	square inches	645.2	square millimeters	mm^2
ft^2	square feet	0.093	square meters	m^2
yd^2	square yard	0.836	square meters	m^2
ac	acres	0.405	hectares	ha
mi^2	square miles	2.59	square kilometers	km^2
		VOLUME		
fl oz	fluid ounces	29.57	milliliters	mL
gal	gallons	3.785	liters	L
ft^3	cubic feet	0.028	cubic meters	m^3
yd^3	cubic yards	0.765	cubic meters	m^3
		NOTE: volumes greater than 1000 L shall be shown in m^3		
		MASS		
oz	ounces	28.35	grams	g
lb	pounds	0.454	kilograms	kg
T	short tons (2000 lb)	0.907	megagrams (or "metric ton")	Mg (or "t")
		TEMPERATURE (exact degrees)		
°F	Fahrenheit	5 (F-32)/9 or (F-32)/1.8	Celsius	°C
		ILLUMINATION		
fc	foot-candles	10.76	lux	lx
fl	foot-Lamberts	3.426	$candela/m^2$	cd/m^2
		FORCE and PRESSURE or STRESS		
lbf	poundforce	4.45	newtons	N
lbf/in^2	poundforce per square inch	6.89	kilopascals	kPa

APPROXIMATE CONVERSIONS FROM SI UNITS

Symbol	When You Know	Multiply By	To Find	Symbol
		LENGTH		
mm	millimeters	0.039	inches	in
m	meters	3.28	feet	ft
m	meters	1.09	yards	yd
km	kilometers	0.621	miles	mi
		AREA		
mm^2	square millimeters	0.0016	square inches	in^2
m^2	square meters	10.764	square feet	ft^2
m^2	square meters	1.195	square yards	yd^2
ha	hectares	2.47	acres	ac
km^2	square kilometers	0.386	square miles	mi^2
		VOLUME		
mL	milliliters	0.034	fluid ounces	fl oz
L	liters	0.264	gallons	gal
m^3	cubic meters	35.314	cubic feet	ft^3
m^3	cubic meters	1.307	cubic yards	yd^3
		MASS		
g	grams	0.035	ounces	oz
kg	kilograms	2.202	pounds	lb
Mg (or "t")	megagrams (or "metric ton")	1.103	short tons (2000 lb)	T
		TEMPERATURE (exact degrees)		
°C	Celsius	1.8C+32	Fahrenheit	°F
		ILLUMINATION		
lx	lux	0.0929	foot-candles	fc
cd/m^2	$candela/m^2$	0.2919	foot-Lamberts	fl
		FORCE and PRESSURE or STRESS		
N	newtons	0.225	poundforce	lbf
kPa	kilopascals	0.145	poundforce per square inch	lbf/in^2

TABLE OF CONTENTS

LIST OF FIGURES

LIST OF TABLES

CHAPTER 1. INTRODUCTION

The Michigan Department of Transportation (MDOT) is investigating a replacement bridge for the existing Lafayette Avenue Bridge over the Saginaw River in Bay City, MI. Like the current bridge, the proposed bridge features two large bascule piers, which may create complex flow patterns due to their wide widths. MDOT calculated the scour depths using the current standard practice, which assumes a uniform layer of bed material, in this case, sand. The scour calculations, however, seemed excessive to MDOT, as they were aware of a thick, subsurface clay layer extending across the entire site channel. Cohesive materials, such as clay, are typically more resistant to scour compared to sandy materials due to higher critical shear stresses, but the critical shear value of cohesive materials is preferable to be obtained through erosion testing (Arneson et al. 2012).

In 2020, the Federal Highway Administration (FHWA) established a Transportation Pooled Fund (TPF) study, TPF-5(461) Soil and Erosion Testing Services for Bridge Scour Evaluations (FHWA 2020). This study is a collaborative effort between the Hydraulics and Geotechnical Research Programs at Turner-Fairbank Highway Research Center (TFHRC) and includes support from the FHWA Resource Center. The study allows State departments of transportation to partner with FHWA to perform the soil and erosion testing required to determine material properties, such as critical shear stress, which are needed to calculate scour depths more accurately. With a potential layer of cohesive material within the calculated scour depth, the Lafayette Avenue Bridge was an excellent candidate for this TPF study. The study also aligns with FHWA's NextScour research initiative, which seeks to improve scour analysis and provide more accurate scour depth estimates for foundation design (Shan et al. 2021a).

In addition to providing soil erosion testing, researchers at the FHWA J. Sterling Jones Hydraulics Research Laboratory proposed to model the flow around the Lafayette Avenue Bridge's wide bascule piers. The Hydraulics Laboratory researchers have extensive experience conducting computational fluid dynamics (CFD) modeling, which can capture the complex three-dimensional (3D) flow at the piers. The team also proposed conducting physical modeling of the bridge piers and abutments using flume testing to calibrate and verify the CFD models. Additionally, both the laboratory and FHWA Resource Center personnel could help verify the traditional one- and two-dimensional (1D and 2D) hydraulic modeling performed for the site.

The Hydraulics Laboratory team presented a study approach on October 15, 2020, to MDOT, which contained the following five tasks:

- Task 1. Hydraulic modeling to obtain the representative initial bed shear stress.
- Task 2. Erosion testing to obtain the distribution of clay critical shear stress.
- Task 3. Decay functions, developed from the flume test and CFD shear stresses, to model the hydraulic loading.
- Task 4. CFD scour to model the scour progress in clay and sand.
- Task 5. Probabilistic scour analysis to develop probabilistic distributions of the maximum scour depths considering the uncertainties from the flood discharge, roughness on the main channel and the floodplain, and soil erosion resistance.

This report references measurements and calculations in both English and International System of Units (SI). References to bridge plans, hydraulic analysis, and geotechnical studies typically use English units. References to laboratory equipment, laboratory tests, and CFD modeling typically use SI units. Conversions from SI to English units are provided when appropriate.

CHAPTER 2. PROJECT BACKGROUND

The Lafayette Avenue Bridge carries SR M-13 and SR M-84 over the east channel (or main channel) of the Saginaw River in Bay City, MI. The west abutment rests on Middle Ground Island, and a second fixed bridge connects to Salzburg Avenue over the smaller west channel of the river. Originally opened in 1938, the Lafayette Avenue Bridge features two bascule piers that support a 184-ft-long bascule span. The bridge was rehabilitated in 1987 to replace the superstructure, but the existing substructure was retained.

MDOT's newly proposed bridge, shown in figure 1, will replace the entire substructure and superstructure in the current location of the existing bridge. The proposed piers are larger than the current piers and are spaced farther apart to maintain a bascule span distance of 190 ft. Both the proposed left and right abutments are set further back into the embankment compared to the original abutments to provide additional relief to the main channel. The proposed left abutment is a spill-through abutment, while the right abutment is a vertical-wall abutment carrying a pedestrian path under the approach span. The proposed foundations feature H-piles support for all piers and abutments. In addition to the H-piles, MDOT plans on installing cofferdams around the perimeter of each pier to protect the piles.

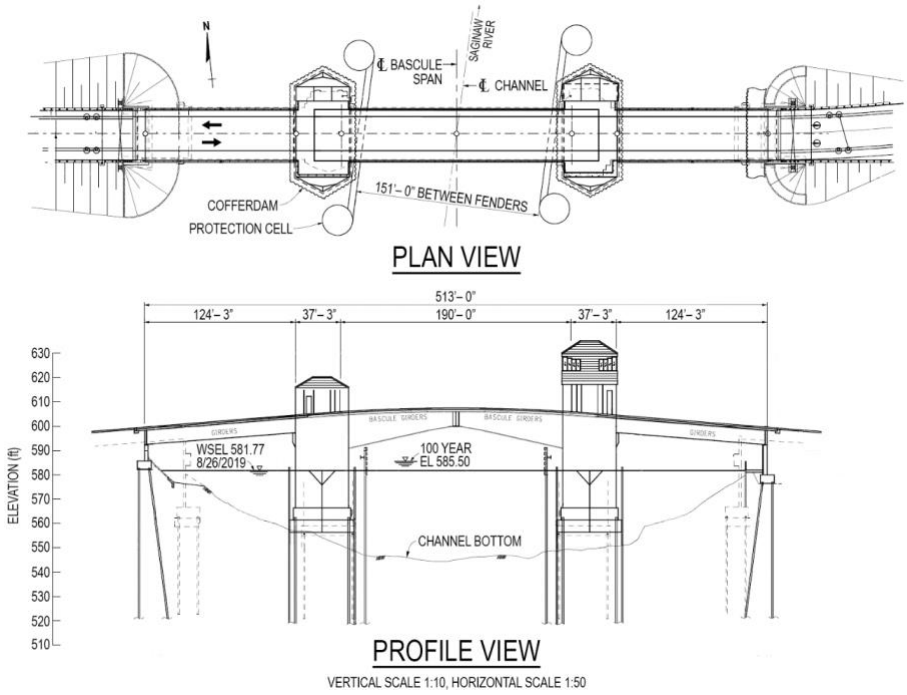

Figure 1. Schematic. Plan and profile views of the proposed Lafayette Avenue Bridge.

To protect the bascule piers from passing vessels, MDOT plans to install a fender system with a 151-ft clearance between the piers. Each fender features a 25-ft-diameter cell up and downstream of the pier. The fender channel is aligned with the main channel of the Saginaw River and is at a slight 7.5-degree skew with the centerline of the deck and the bascule span.

SUBSURFACE SOIL PROFILE AND GEOTECHNICAL PROPERTIES

The subsurface soil profile at the site was determined from a 2016 geotechnical site investigation conducted by MDOT. Five soil borings were conducted in the floodplain surrounding each abutment. Sediment probes were conducted upstream and downstream of each pier, as well as two additional borings in the channel. The investigation revealed that the subsurface soils at both overbanks had an initial layer of fill consisting of loose sand and silt, followed by a layer of decomposed wood, sawdust, sand, and silt, with traces of gravel. The right overbank then transitioned to a 15-ft-thick layer of poorly graded sand. The left overbank (part of Middle Ground Island) was found to have silt and sand layers at this level. Starting at an elevation of around 553 ft in the right overbank and around 533 ft in the left overbank, the soil profile transitioned to a thick layer of stiff, gray, lean clay that continued down to an elevation of 485 ft, where it reached a layer of shale.

The main channel bed featured a thin layer of river sediment that consisted of clayey/sandy silt. MDOT found the corresponding median grain size (D_{50}) of this fine silty sand to be 0.1 mm. Beneath the sediment was the layer of poorly graded, loose sand and silty sand, which varied in thickness between 5 and 10 ft. Between elevations 533 and 540 ft, the sand layer transitioned to the thick layer of lean clay. The borings suggested that this clay layer was continuous across the entire profile of the channel. A generalized subsurface profile at the center line of the existing bridge was created using the boring data and is shown in figure 2.

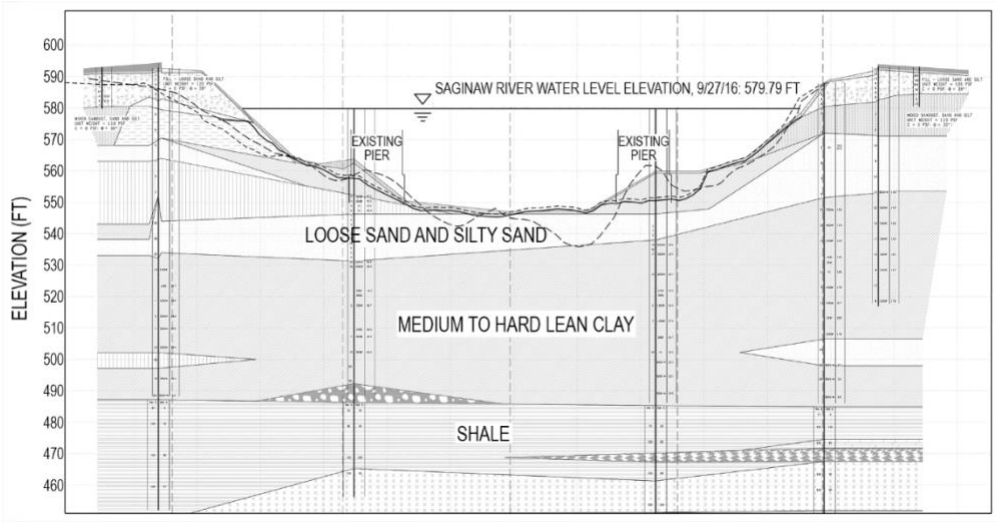

Figure 2. Schematic. Subsurface profile of the bridge site.

The clay layer started out very stiff at the right overbank, with standard penetration tests (SPTs) producing blow counts (*N*-values) of 30 blows per ft at an elevation of 550 ft. These values dropped quickly to around 10 blows per ft at an elevation of 540 ft. Beginning at this depth, the clay experienced similar *N*-values across the entire profile of the channel, varying between 7 and 12 before increasing again near the shale layer. MDOT believed that this thick layer of lean clay could potentially provide sufficient erosive resistance to the design floods and reduce the original values of the design scour depths.

SUMMARY OF CURRENT HYDRAULIC ANALYSIS

MDOT prepared a hydraulic scour report to calculate scour depths for the proposed bridge. The hydrological analysis determined a drainage area of 6119.5 mi^2, and Q_{100} and Q_{500} flow discharges of 56,770 and 67,740 cubic ft per second (cfs), respectively.

The flow parameters at the bridge site were calculated using the U.S. Army Corps of Engineers (USACE) Hydrologic Engineering Center's River Analysis System (HEC-RAS) software (USACE 2022). The model considered 12 cross sections in the west channel of the Saginaw River, 13 cross sections in the east channel (including the cross section of the proposed Lafayette Avenue Bridge), and 3 cross sections in the combined lower reach. The HEC-RAS model considered a Manning's n value of 0.030 for the main channel and varied between 0.06 and 0.14 in the left and right overbanks. HEC-RAS returned an average velocity at the cross section directly upstream of the bridge of 5.27 ft/s and a hydraulic depth of 23.80 ft for the Q_{100} flow and 6.10 ft/s and 24.29 ft for the Q_{500}.

The material in the riverbed was very fine sand with a D_{50} of 0.1 mm. Using the methodology from Hydraulic Engineering Circular No. 18 (HEC-18), the calculated critical velocity of the bed material was less than the mean velocity in the channel for the Q_{100} discharge, indicating that Laursen's live-bed scour equation should be used to calculate contraction scour (Arneson et al. 2012). The predicted contraction scour depth was rounded to 5 ft for the Q_{100} flow and 6 ft for the Q_{500}.

Local scour was also calculated at the piers using HEC-18 methodology. The proposed pier geometry and the flow parameters were entered into the pier scour equations, and a correction factor was applied to account for the wide piers in shallow flow. The resulting pier scour depths were 31 ft for the Q_{100} flow and 35 ft for the Q_{500}. Local scour equations for the proposed abutments predicted flow would remain in the main channel and that zero abutment scour would occur for either flow.

The total scour calculation combined the contraction and pier scour values and resulted in a 36-ft scour depth for the Q_{100} flow and 41-ft scour depth for the Q_{500}. Considering an average channel bed elevation of 550 ft, these scour depths corresponded to elevations of 514 and 509 ft, respectively. For comparison, the clay layer at the site began at elevations between 530–540 ft.

In addition to the conventional hydraulic analysis, 6 mi downstream of the bridge is the Saginaw Bay, which is part of Lake Huron. Although the Great Lakes do not experience coastal tides, the water elevation on the lake can fluctuate due to seiches, which are standing waves produced by wind and atmospheric pressure. If the crest of a standing wave recedes at the river outlet, it could potentially lower the water surface elevation (WSE) at the downstream boundary of the HEC-RAS model. Lower water surface elevations could produce increased velocities at the bridge site. Fluctuating boundary conditions at the bridge site due to lowering lake water elevation levels were a subject for further investigation in the study.

CHAPTER 3. TASK 1. HYDRAULIC MODELING

Hydraulic modeling for this study aimed to predict the flow depths, velocities, and bed shear stresses at the bridge. This task used a 2D riverine and 3D coastal model to study the complex flow at the bridge site that is influenced by the Middle Ground Island dividing the Saginaw River into two channels, a river confluence near the south end of the island, and water level fluctuations of Lake Huron several miles downstream. Data from the 2D riverine and 2D/3D coastal model established the boundary conditions for the CFD model that included an area approximately 1,000 ft upstream and downstream of the bridge. The CFD model computed bed shear stresses in the bridge opening and around the proposed bascule piers.

The 3D CFD model was developed by combining the light detection and ranging (LiDAR) topography (exported from the Sedimentation and River Hydraulics – Two Dimension (SRH-2D) model from MDOT) and the computer-aided design (CAD) model of the proposed bridge (U.S. Bureau of Reclamation 2022). Multiple flow conditions were simulated, including the Q_{100} and Q_{500}. CFD simulation focused on the region around the bridge (figure 3).

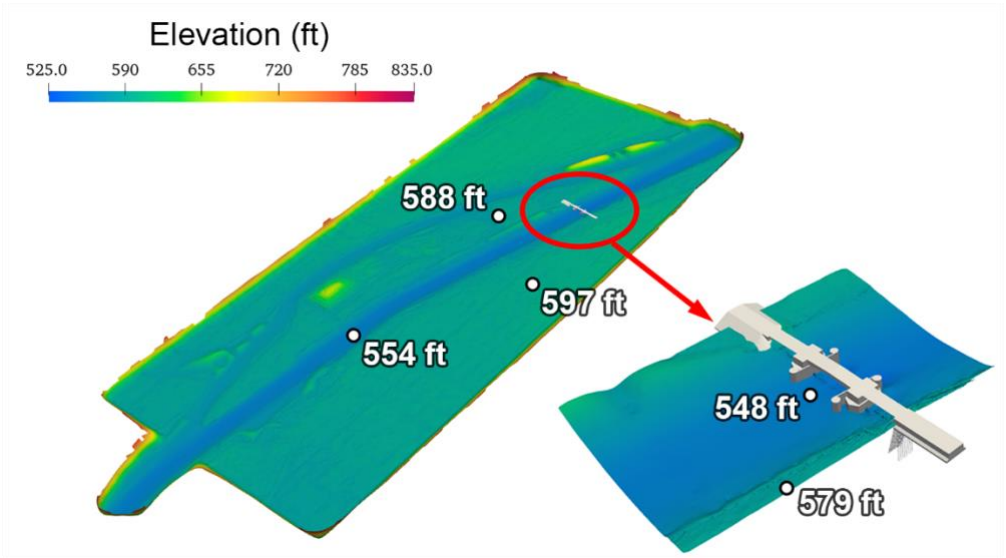

Source: FHWA.

Figure 3. Image. LiDAR topography and the CFD simulation domain with the proposed bridge model.

A volume of fluid (VOF) model was first evaluated, which simulated two-phase flow (air and water) in a 3D volume to better predict the water surface elevation. The inlet boundary was set as a uniform velocity inlet, and the outlet boundary was set as a pressure outlet. The riverbed was modeled as a rough wall with a roughness height of two times the riverbed surface sand D_{50}. Corresponding single-phase models were developed to simplify the simulations. A CFD single-phase model does not incorporate air in the simulation. Instead, a top wall is placed at the expected water surface elevation (obtained from the HEC-RAS model). It is set as a symmetrical boundary to simulate the water surface. The inlet was set as a flow rate inlet, while the outlet boundary and riverbed were identical to the VOF model. The Unsteady Reynolds-Average

Navier-Stokes (URANS) solver with a *k*-epsilon turbulence model was selected to solve the momentum equations.

Initial test runs showed that the VOF and single-phase models produced similar results, so the single-phase model was adopted for the remaining CFD simulations. The simulation results of flow velocities and bed shear stresses of the single-phase model were compared with SRH-2D results. As shown in Figure 4, velocity distributions between both models were similar. The upstream approach velocity in each case was almost the same. But the water flow around the piers was different in the SRH-2D model because it cannot accurately simulate the 3D flow pattern around the bridge. Figure 5 compares the bed shear stresses. The SRH-2D model showed relatively larger bed shear stresses upstream and downstream of the bridge compared to the CFD model but had comparable stresses closer to the bridge.

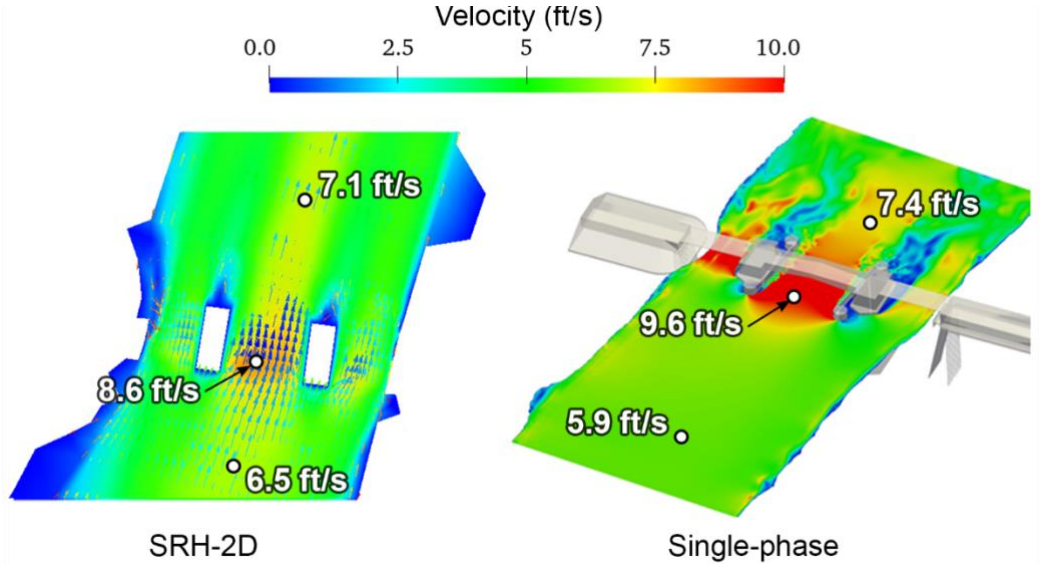

Source: FHWA.

Figure 4. Image. Velocity distributions of SRH-2D and the single-phase model.

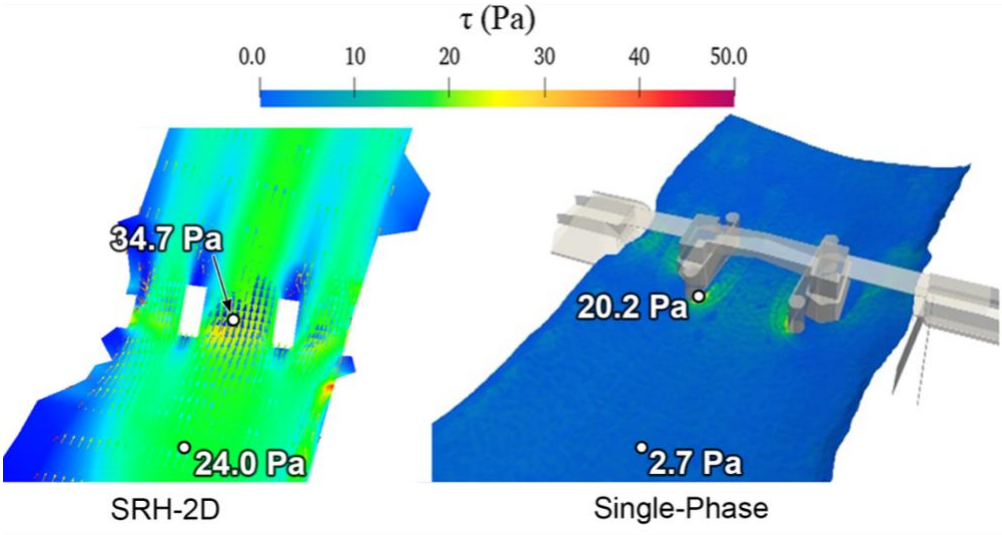

Source: FHWA.
1 Pa = 0.021 lb/ft^2 (psf).

Figure 5. Image. Bed shear stress distributions of SRH-2D and the single-phase model.

NOMINAL CFD BED SHEAR STRESS

The riverbed in a CFD model is composed of millions of cells, with each cell outputting a single shear stress value. In order to determine a relevant average shear stress value adjacent to the bridge pier, an area of interest must be identified. Then the shear stress values from cells in that area can be averaged. A flow separation zone forms when water passes an obstruction. Bed shear stresses in the separation zone are amplified compared to upstream approach shear stresses, which initiate the scour process. CFD simulation results indicated that the flow separation zone is similar in size to the blockage area due to the obstruction. The blockage area is equal to the obstruction width times the flow depth. Therefore, the flow separation zone is the area of interest, where bed shear stresses are averaged to determine the representative shear stress due to the obstruction. This averaged representative bed shear stress can then be compared to shear stresses calculated from HEC-RAS output flow parameters to complete the probabilistic scour analysis in Task 5, which is discussed in chapter 7.

For the Lafayette Avenue Bridge, the proposed upstream fender would have the deepest scour hole, where the blockage area was considered the fender diameter times the flow depth. Because the piers were close to the river banks, only bed shear stresses from cells adjacent to the bridge pier and elevations below the pier pile cap were collected. The shear stresses were ranked from largest to smallest until the cumulative cell area equaled the blockage area. Area-weighted average shear stress was then calculated to be the nominal bed shear stress. Table 1 lists the nominal shear stresses at the two fenders for increasing flows.

Table 1. Flow conditions and representative shear stresses for different flows.

Flow	Flow Rate (cfs)	WSE (ft)	Average Velocity (ft/s)	Blockage Area (ft^2)	Shear Stress at Left Fender (Pa)	Shear Stress at Right Fender (Pa)
Q_{10}	42,785	580.9	4.4	865.7	8.2	7.1
Q_{50}	54,510	581.3	5.5	875.7	12.1	11.6
Q_{100}	59,360	581.5	5.9	880.5	14.5	14.1
Q_{500}	70,130	582.0	6.8	893.2	20.2	19.7
Q_{2000}	79,295	582.3	7.5	899.3	26.2	24.5

CHAPTER 4. TASK 2. EROSION TESTING

MDOT collected 27 Shelby tube soil samples in three boreholes at the bridge site. The first two boreholes were downstream of the bridge at each of the existing piers (BB101 and BB102), and the third borehole was located at the left abutment upstream of the bridge (MB1). MDOT shipped the Shelby tubes to the Hydraulics Laboratory at TFHRC for erosion testing using the Ex-situ Scour Testing Device (ESTD). Figure 6 shows the Shelby tube sampling depths with the nine tubes tested in the ESTD highlighted. The erosion testing results determined a critical shear stress distribution of the medium-to-hard lean clay layer and was later used for the probabilistic scour analysis discussed in Task 5 in chapter 7.

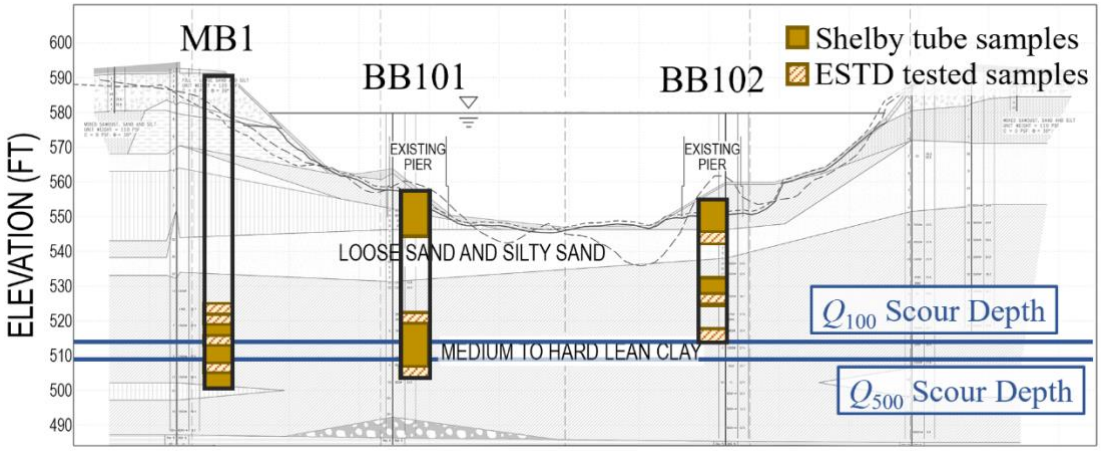

Figure 6. Drawing. Locations and elevations of MDOT Shelby tube samples.

ESTD SUMMARY

The ESTD, shown in figure 7, is an automated erosion device developed by FHWA that measures the erodibility of a cylindrical soil sample under well-controlled flow conditions (Shan et al. 2011). The ESTD features a 4.7-inch wide by 0.75-inch-high rectangular acrylic test channel that is 3-ft long. The maximum flow capacity of the pump is 0.5 cfs, which translates to a maximum flow velocity of 20 ft/s. An underwater laser scanner mounted on an industrial robotic arm scans the soil surface every 20 s (figure 8), sending a quasi-instantaneous signal to the control program. The control program averages the scan data and compares it to a reference point on the surface of the test channel. If the average value is less than this reference point, a command is sent to the piston to extrude the sample to maintain the soil surface flush with the test channel bed. The control program records the extrusion data from the piston, which is used to calculate the erosion rate. Flow circulation is continuously measured using an electromagnetic flow meter, and two filtration tanks are used to capture the eroded clay particles and keep the water clear for the laser scanner. An electromagnetic shear sensor located just upstream of the piston directly measures the shear stress of the soil sample in a separate series of tests after erosion testing is completed. The relationship between erosion rates and shear stresses was developed by comparing results at similar flow rates, which is then used to determine the critical shear stress of the soil. Shan et al. (2021b) outlined in detail the ESTD test procedures.

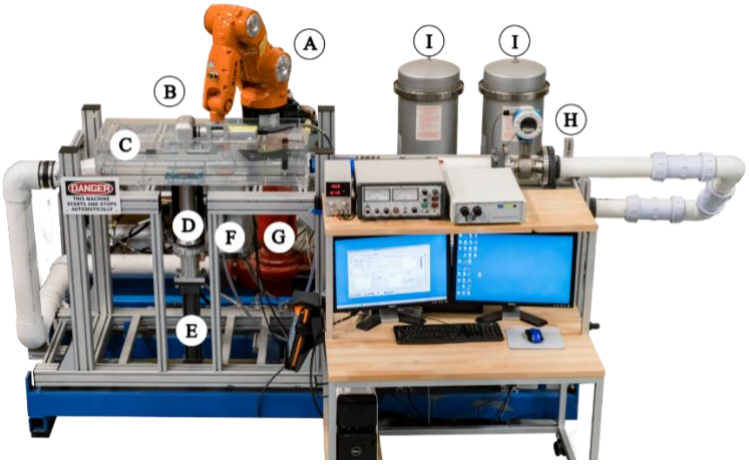

Source: FHWA.

A = robotic arm; B = laser scanner; C = flow channel; D = 3-inch Shelby tube sample; E = hydraulic piston; F = shear sensor; G = flow pump; H = flow meter; and I = filter cylinders.

Figure 7. Photo. Labeled parts of the ESTD.

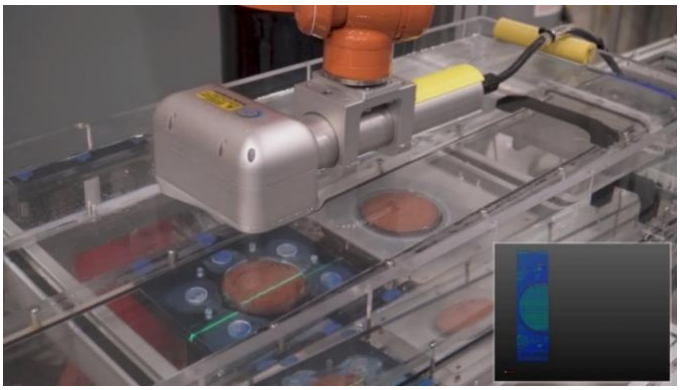

Source: FHWA.

Figure 8. Photo. The laser scanner measuring the soil surface and digitized soil surface (inset).

For ESTD erosion tests, one or two 1-ft sections were cut from each Shelby tube, usually from the tube bottom. On top of each tube sample, lab engineers performed the rapid strength tests using a pocket penetrometer (PP) and a vane shear tester. After extracting and removing the disturbed soil surface from these strength tests, lab engineers conducted erosion tests on the remaining soil in the tube. Only the top 9–10 inches of soil were tested because the bottom 2–3 inches had a greater propensity to dislodge from the tube in the flow due to decreased friction surface area between the soil and the Shelby tube. Table 2 shows the elevation ranges of ESTD test tubes, strength test results, and water content of each Shelby tube sample. FHWA's Geotechnical Laboratory provided soil classifications for three of the tested samples, including MB1 ST1, MB1 ST2, and BB102 ST14, and determined they were all low-plasticity clay. They then tested an additional six samples not included in ESTD erosion testing and found those were also all classified as low-plasticity clay.

The typical duration of an erosion test for one flow rate/velocity setting was 10 min. A linear best fit line was applied to the erosion data (recorded position of the soil surface versus time) for each flow rate, where the slope represented the erosion rate. Hydraulic shear stresses on soil samples were recorded separately from the erosion tests using 0.6-inch-thick soil samples confined in stainless steel rings. The ring is mounted to a small bowl that attaches directly to the sensor disk. The bowl's interior features a raised circular platform, which pushes the soil out about 0.08 inches above the edge of the ring. After the ring is mounted on the shear sensor, the sensor disk height is adjusted until the soil surface is flush with the test channel surface. The shear stress data were used to convert flow rates into equivalent shear stress values.

Table 2. Elevations of ESTD erosion test samples and basic soil geotechnical information.

Tube Number	Elevation (ft)	Elevation of 1-ft Test Tube (ft)	Elevation of Strength Test (ft)	PP (kPa)	Vane Shear Strength (kPa)	Water Content (percent)
MB1 ST1	526.1-523.6	524.6–523.6	524.7	119.7	64	8.7
MB1 ST2	523.6-521.1	522.1–521.1	523.2	105.3	40	13.6–14.9
MB1 ST4	518.6-516.1	517.1–516.1	518.2	143.6	48	20.5–23.4
MB1 ST8	508.6-506.1	507.2–506.2	507.2	71.8	36	28.2–29.8
BB101 ST12	522.1-520.1	520.8–519.8	520.7	80	22	14.9
BB101 ST15	507.6-505.1	507.1–506.1	507.1	76.5	44	23.5
BB102 ST5	542.9-540.4	541.9–540.9	540.9	57.5	40	28.2
BB102 ST11	527.9-525.4	526.5–525.5	526.5	167.6	86	14.9–17.7
BB102 ST14	517.9-515.4	517.9–515.4	516.6	167.6	62	26.6

ST = Shelby tube; 1 kPa = 21 psf.

ESTD EROSION DATA ANALYSIS

Generally, the soils within all nine Shelby tube samples had higher erosion rates as the flow rates increased, i.e., increased shear stresses, as shown in figure 9. Figure 9 also revealed that Shelby tubes ST5 and ST14 from borehole BB102 had much higher erosion rates at the same shear stresses than other tubes, indicating lower critical shear stresses for these two tubes. Figure 10 shows the erosion data in log-log scale along with the erosion categories proposed by Briaud (2011). Outside of ST5 and ST14, most data points fall within the low erodibility category. Because of data scatter in figure 9 and figure 10, it was very difficult to fit the data using a single curve. Therefore, alternative methods were considered to derive a shear stress distribution for the entire clay layer instead of only finding a deterministic value of the critical shear stress value.

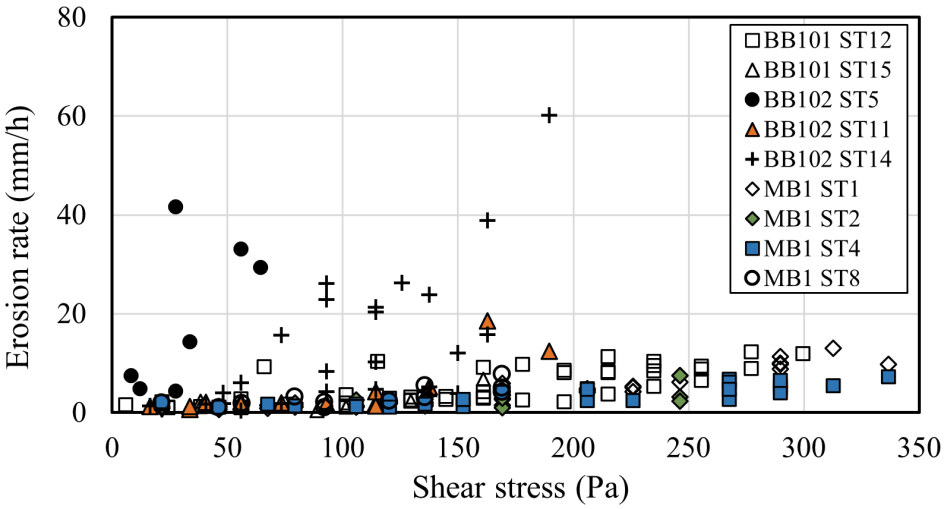

Source: FHWA.

Figure 9. Graph. Erosion rates of nine tested Shelby tube samples.

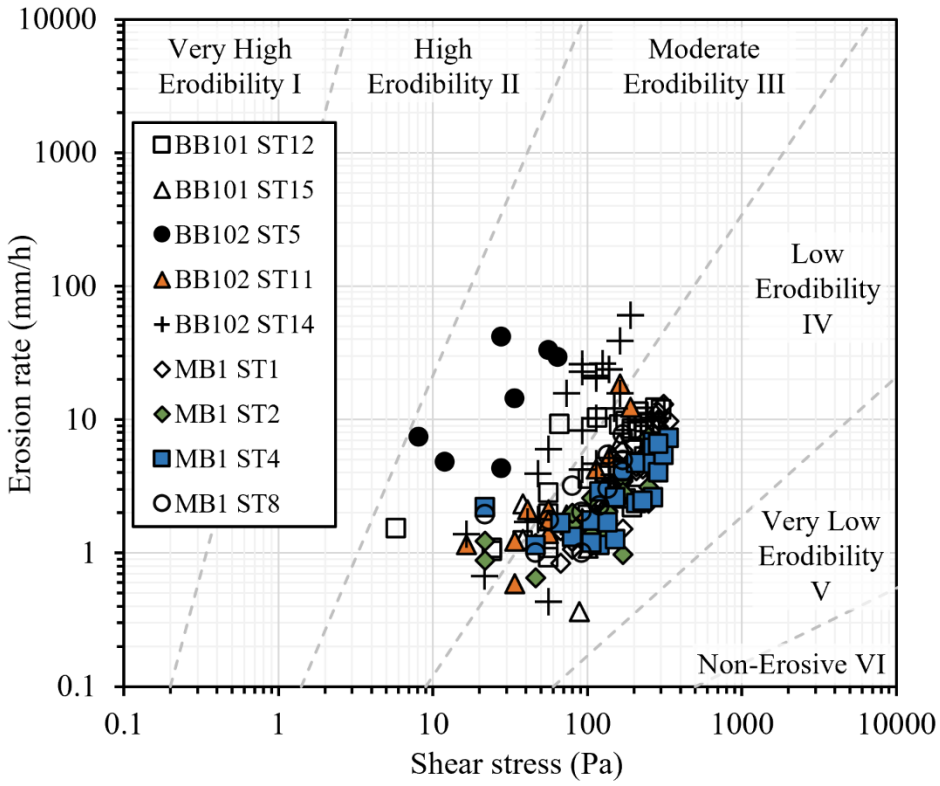

Source: FHWA.
Note: Dashed lines represent boundaries of erosion categories.

Figure 10. Graph. Erosion rates of samples with corresponding erosion categories.

CRITICAL SHEAR STRESS DISTRIBUTION

Because the ESTD can produce a wide range of flow rates and erosion rates, a probabilistic analysis method was considered to determine the critical shear stress value along with a confidence interval, which is typically expressed as a coefficient of variation (COV). FHWA considered multiple methods to determine these values. Before any method was applied, the data were broken down into smaller time windows. It is not unusual during the 10-min erosion test for the soil to erode at different rates throughout the run. The simplest method to interpret the erosion rate was to calculate a best fit line across the entire length. But if the data are broken down into smaller time windows, varying from 1–4 min, with overlaps of 50 percent, more data points are generated that better represent the full range of erosion seen in the original 10-min run.

There were two methods considered for determining the critical shear stress of the soil using a probabilistic analysis. The first method was the bin method. The set of data points was separated into a series of horizontal bins containing a certain range of erosion rates, where the total number of bins was equal to the log-base 2 value of the number of datapoints. Each bin contained an equal amount of data points. For each bin, the mean, standard deviation, and COV were calculated for both erosion rates and shear stress values. Then the mean values were plotted and fitted using the erosion power function to find a resulting critical shear stress.

The second method was the bootstrapping method (Stine 1989). In this method, the data are plotted on a log-log plot, and from the cloud of data points, a subset is selected at random. From this subset, a log-log best fit line is calculated. This process is repeated *N* number of times, anywhere from 5,000 to 50,000. For this method, a nonzero erosion rate must be selected to find the critical shear stress value, typically 0.1 mm/h (0.0039 inch/h), which matches the definition used by Briaud et al. (2011). The intersection of the best fit lines at the selected erosion rate results in a distribution of critical shear stress values from which a COV can also be calculated. Both methods were tested by FHWA to evaluate the optimal way to determine the probabilistic distribution of critical shear stress values for a tested soil. The bootstrapping method was eventually selected because it generated more reliable and reproducible distributions from the erosion datasets.

The first step of the bootstrapping method was to apply a power function to describe the erosion function of the cohesive soil tested as follows:

$$\dot{e} = k_a \tau^{k_b} \quad (1)$$

Where:

$\dot{e}$ = erosion rate.
τ = shear stress.
k_a, k_b = equation constants.

By taking the logarithm of both sides, equation 1 converts to a linear relationship (as shown in equation 2), and a linear best fit was applied to the data to obtain constants k_a and k_b. After fitting both constants, the critical shear stress was defined as the shear stress when the erosion rate equaled 0.1 mm/h, as follows:

$$\log(\dot{e}) = \log(k_a) + k_b \times \log(\tau) \quad (2)$$

The erosion data were divided into 4-min time windows, with 2-min overlaps between adjacent windows. A linear best fit function was applied to each window, where the slope of the linear fit was equal to the erosion rate. For very low flows, where erosion may not be detectable by the laser, a lower boundary for erosion was set at 0.016 mm/h (6.3×10^{-4} inch/h), which was based on the resolution of the laser scanner. In total, 1,127 erosion data points were collected (figure 11). The solid line represents the linear fit function for the entire dataset. With the corresponding fitted constants k_a of 0.00033 and k_b of 1.89, the critical shear stress was calculated to be 20.5 Pa (0.431 psf).

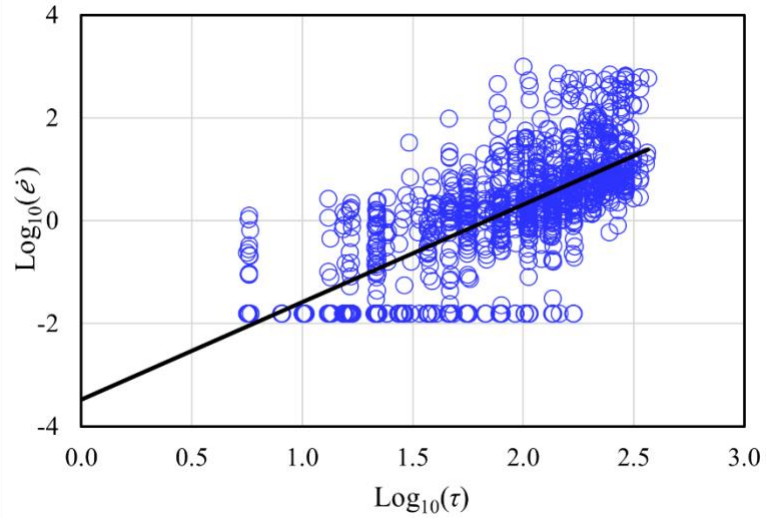

Source: FHWA.

Figure 11. Graph. Logarithmic best fit of the erosion data.

The second step of the bootstrapping method was to randomly select a subset of data points from the total set and apply the logarithmic best fit equation. A script randomly selected 40 out of the 1,127 total data points and then applied the best fit function to calculate a corresponding critical shear stress. This process was then repeated 50,000 times to get a distribution of critical shear stresses (figure 12). The two dashed lines represent the 95-percent confidence limits on the linear fit of the mean critical shear stress, and the solid line is the mean linear fit of the 50,000 iterations. Figure 13 plots a histogram of all 50,000 critical shear stresses. The mean value of the critical shear stresses was 20.5 Pa (0.431 psf), which matched the value calculated previously for the entire 1,127-point dataset. The standard deviation was 6.56 Pa (0.138 psf), and the coefficient of variation was 0.32. Both mean and COV were used as the critical shear stress distribution parameters. Since the erosion rates follow a lognormal distribution, the distribution of the critical shear stress was also assumed lognormal.

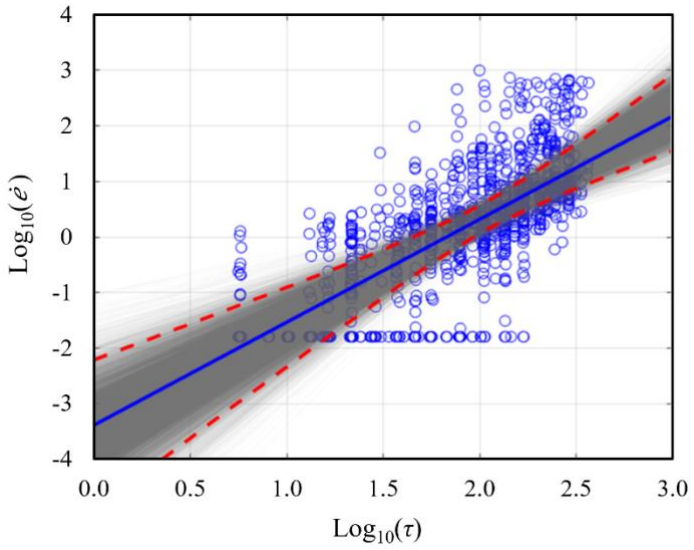

Source: FHWA.

Note: Dashed lines represent the 95-percent confidence interval on the mean linear fit.

Figure 12. Graph. Bootstrapping technique showing 50,000 linear fittings.

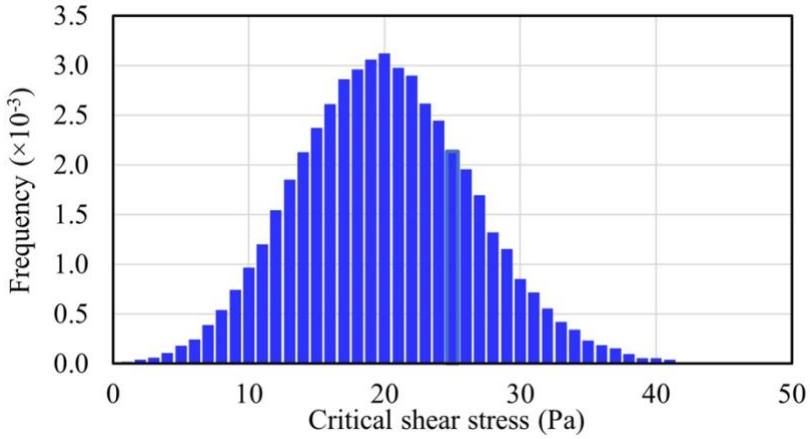

Source: FHWA.

Figure 13. Graph. Histogram of the 50,000 critical shear stresses.

CHAPTER 5. TASK 3. DECAY FUNCTIONS

Physical experiments were conducted in the Hydraulic Laboratory's 6-ft-wide Multi-functional Flume System (MFS) using scaled Lafayette Avenue Bridge models to understand where scour holes would form and the depths they would reach. Multiple model configurations were tested, including pier with embankment and abutment. Flume tests ran for 70 h minimum, but could last up to 120 h, and were paused at regular intervals to scan the bathymetry to measure the incremental progress of the scour hole. These scans were then used to calculate the decay of the hydraulic loads and calibrate the computer models of the experiments.

FLUME SCOUR TESTS

The Froude criterion was used to determine the geometric scale of the model because the governing force is gravity and open channel flow aspects dominate. A geometric scale factor (model:prototype) of 1:50 was selected for the flume tests, which provided a reasonable experimental flow depth and an appropriate model size of the bridge components without significant influence from the flume sidewalls. At this scale, the entire bridge was separated into two models: (a) Set L: left half-bridge with pier and abutment, and (b) Set R: right half-bridge with pier and abutment. The model pier was about 1.1 ft wide, and the model fender cylinder had a diameter of 6 inches. The prototype river cross sections were simplified and reproduced in the MFS. Four cross sections upstream of the bridge, two cross sections at the bridge, and five cross sections downstream of the bridge were exported from the LiDAR topography. The average riverbed elevation from these cross sections was 550.2 ft. The averaged left and right bank slopes were 0.13 and 0.22, respectively, with a standard deviation of 0.03.

Figure 14 shows the simplified and scaled model setups in the MFS looking downstream. The 7.5-deg skew angle was kept in the scaled models. The floodplain at the left abutment had an elevation of 576.3 ft. The horizontal distance between the main channel edge and the left floodplain edge measured approximately 154.6 ft. This geometry resulted in a left bank slope of 0.169. Similarly, the right floodplain had an elevation of 582 ft, which resulted in a right bank slope of 0.25. For both sets L and R, a minimum distance of 2 ft was maintained between the fender and the MFS wall to minimize any contraction effects between both.

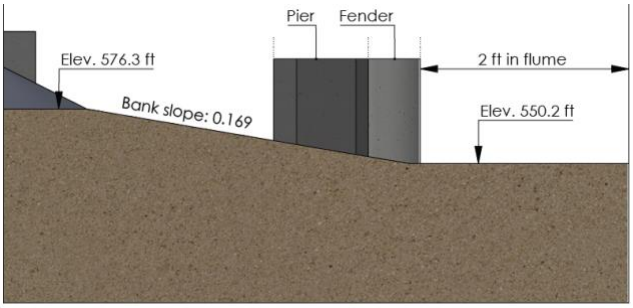

Source: FHWA.

A. Left half bridge.

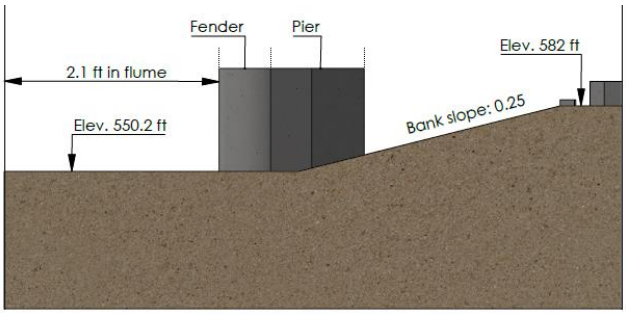

Source: FHWA.

B. Right half bridge.

Figure 14. Image. Scaled bridge models in MFS.

Since both test setups were part of a compound channel, two transition structures were designed and 3D-printed to ensure the rectangular channel smoothly transitioned to the compound channels without introducing scour at the very upstream of the sand recess section. Both sets modeled half of the bridge, but the two models were not split from the centerline of the main channel. Therefore, the flow rate percentage of Q_{100} was estimated from the CFD simulation of the full-scaled geometry. The flow rate ratio of Sets L and R was 64.1 and 59.4 percent, respectively, indicating that the two model sections partially overlapped at the center of the channel.

The Saginaw River bed has very fine sands with a D_{50} of 0.1 mm (0.0039 inch), which are impossible to scale down in flume tests. Uniform sands with a D_{50} of 1.15 mm (0.045 inch) were used instead. The flume-scale flow rate, flow depth, and upstream approach velocity were calculated from the scaling factor, a Q_{100} discharge of 56,770 cfs, and a WSE of 585.5 ft. Table 3 lists the flow conditions. As shown in the table, two different approach velocities were used for each set to ensure the scour depth was accurately measured and the effect of the flume walls was minimized.

Table 3. Flow conditions of flume scour tests.

Cases	Flow Rate (cfs)	Water Depth (ft)	Scaled $V_{Q100,approach}$ (ft/s)	$V_{approach}$ (ft/s)	V Ratio (percent)	Run Time (h)	Scour Depth (ft)
Set L.1	2.1	0.71	0.49	0.49	100	70	0.18
Set L.2	2.5	0.71	0.49	0.58	120	124	0.38
Set R.1	2.1	0.71	**0.45**	0.49	108	87	0.20
Set R.2	2.3	0.71	0.45	0.54	120	85	0.35

The experiment was prepared by positioning the models in the MFS according to the design drawings. The sediment was then placed around the models, compacted by hand, and shaped with the assistance of a robotic arm mounted on a linear carriage over the MFS. The robotic arm could be programmed to repeatedly form complex sediment formations, which included the channel slope.

Each experiment started by scanning the initial bathymetry using an underwater laser scanner. Water was slowly introduced into the flume with a near-zero flow rate to minimize disturbance of the bed material. The flow depth was then increased until the scanner was submerged. Once the laser scan was completed, the experiment began by decreasing the flow depth while gradually increasing the flow rate. Each test required two runs. The first run established the equilibrium scour depth, and the total run time was logged in table 3, and the final bathymetry was scanned. Then a second run was repeated and paused at approximately 20, 40, 60, and 80 percent of the equilibrium scour depth. When the targeted scour depth was reached, the flow was reduced to standing water, and then the laser scanner collected the bathymetry. After the scan was finished, the flow resumed, and the run continued until the next incremental scour depth was reached. Figure 15 shows a typical scanned 3D point cloud.

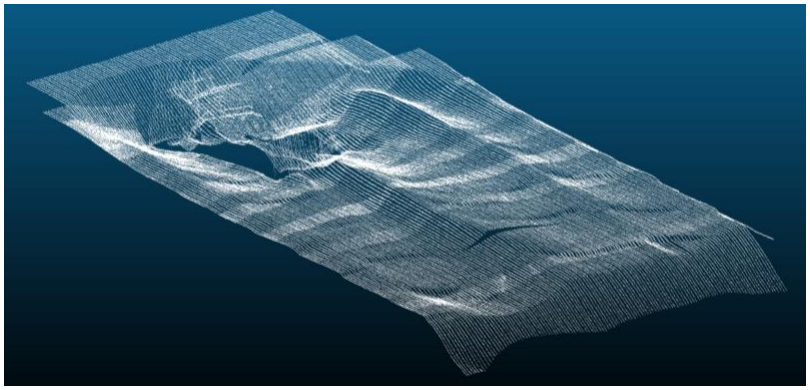

Source: FHWA.

Figure 15. Image. A typical scour bathymetry scanning result.

Figure 16 shows a typical measured scour depth over time, indicating that the scour generally reached equilibrium after about 80 h. Figure 17 shows the equilibrium scour hole around the pier and fender. Water flows from right to left, and the deepest scour hole appears upstream of the upstream fender cylinder.

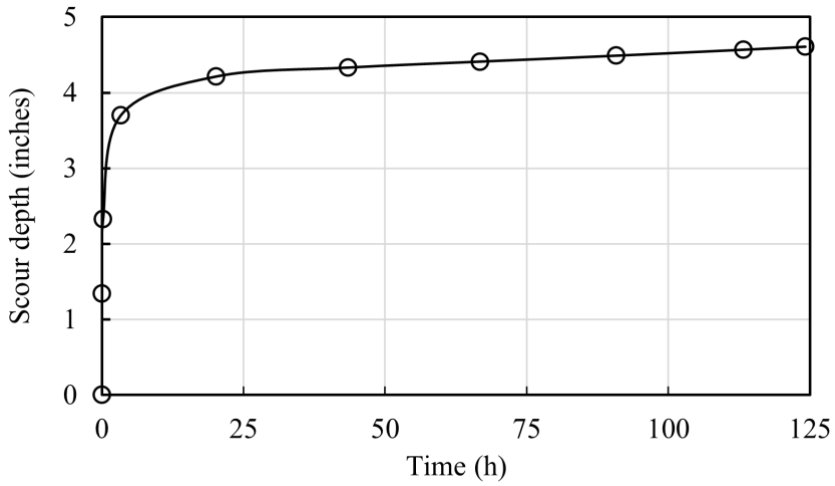

Source: FHWA.

Figure 16. Graph. Scour depths progress of set L.2.

(a) **(b)**

All photos source: FHWA.
Note: Flow is from right to left.

Figure 17. Photos. Final scour hole around: (a) Set L, and (b) Set R.

DECAY FUNCTION DEVELOPMENT

The incremental scour bathymetries collected by the laser scanner were post-processed and exported into CFD to compute the nominal bed shear stress to develop the decay function. The nominal bed shear stress at each incremental scour bathymetry was calculated following the procedure outlined in Task 1. Figure 18 to figure 22 illustrate the bed shear stress distributions for Set L.2 on the scanned incremental scour bathymetries. The figures show that two zones of high shear stress appear on either side of the fender and pier at the initial riverbed. As the scour hole deepens, shear stress magnitude decreases until most of the area around the fender and the pier are lighter intensity, close to the critical shear stress of the 1.15 mm (0.045 inch) sand. This result reflects the trend of shear stress decay within the developing scour hole.

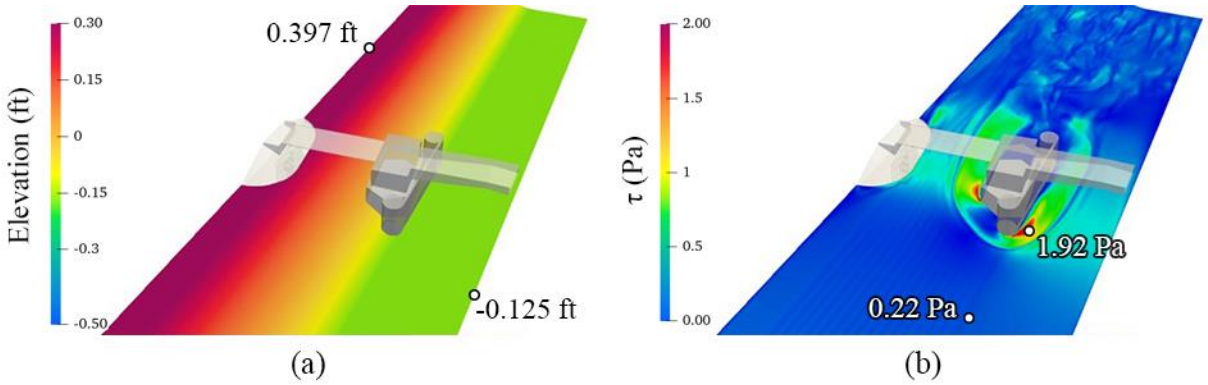

All images source: FHWA.

Figure 18. Image. (a) Experimental bathymetry scan at 0 percent scour depth and (b) resulting CFD bed shear stress distribution.

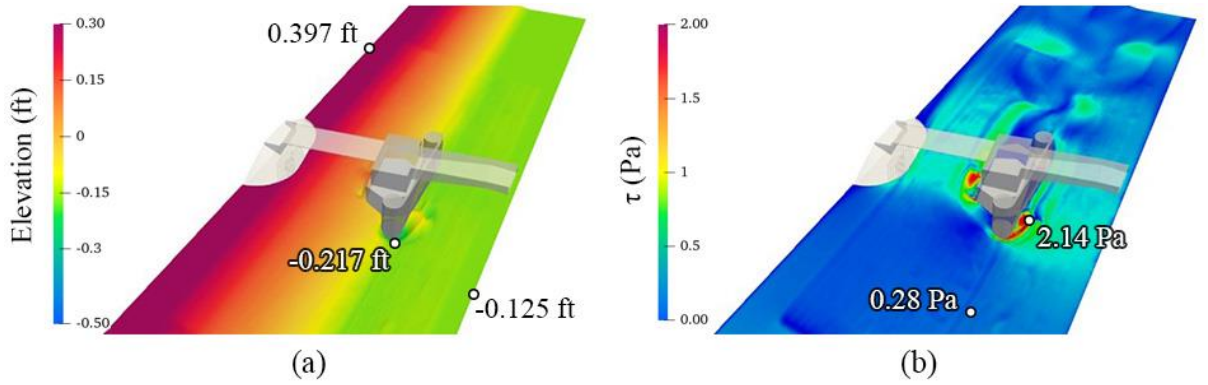

All images source: FHWA.

Figure 19. Image. (a) Experimental bathymetry scan at 21 percent scour depth and (b) resulting CFD bed shear stress distribution.

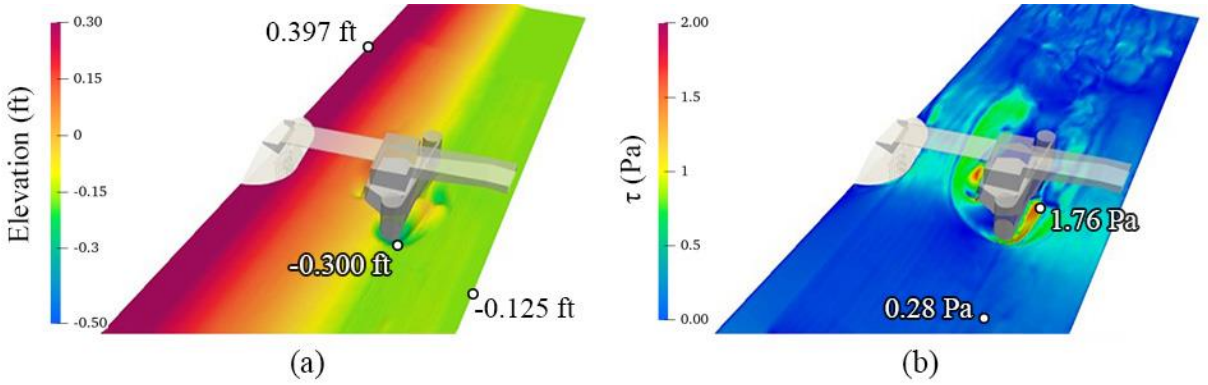

All images source: FHWA.

Figure 20. Image. (a) Experimental bathymetry scan at 51 percent scour depth and (b) resulting CFD bed shear stress distribution.

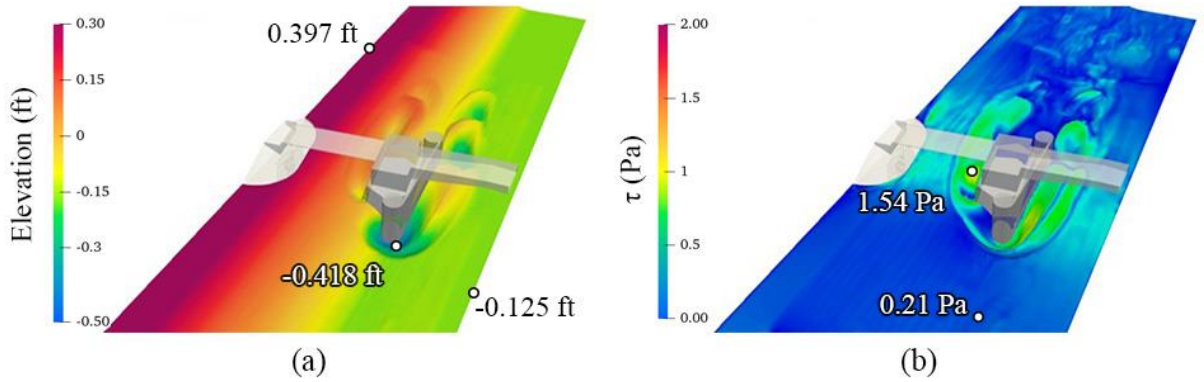

All images source: FHWA.

Figure 21. Image. (a) Experimental bathymetry scan at 81 percent scour depth and (b) resulting CFD bed shear stress distribution.

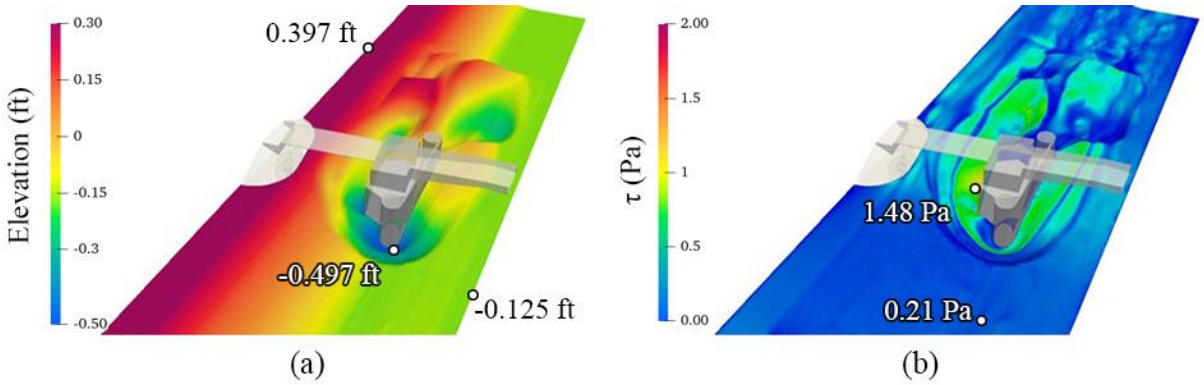

All images source: FHWA.

Figure 22. Image. (a) Experimental bathymetry scan at 100 percent scour depth and (b) resulting CFD bed shear stress distribution.

The representative bed shear stresses at incremental scour depths were normalized by the upstream approach shear stress. Because the flume tests had zero slope, the approach shear stress τ_a was computed using equation 3 with the friction factor f obtained from Moody's Diagram (Moody 1944). Reynolds number and relative roughness were needed to determine the friction factor. For rectangular channels, the characteristic length in Reynolds number is the hydraulic diameter, i.e., four times the hydraulic radius. The relative roughness was assumed as the ratio of $0.5D_{50}$ to the hydraulic diameter.

$$\tau_a = \frac{1}{8} f \rho U^2 \quad (3)$$

Where:

ρ = water density.
U = average approach velocity.

The incremental scour depths were normalized by the obstruction projected width, B, which was used in the Nominal Bed Shear Stress section to calculate the blockage area. Because scour mainly occurs around the upstream fender cylinder for Sets L and R, the projected width was set

as the fender diameter. An exponential function $\frac{\tau}{\tau_a} = a\ exp(-b\ \frac{y_s}{B})$ was fitted through the data for all four cases (figure 23), where y_s is the incremental scour depth, and a and b are fitting constants.

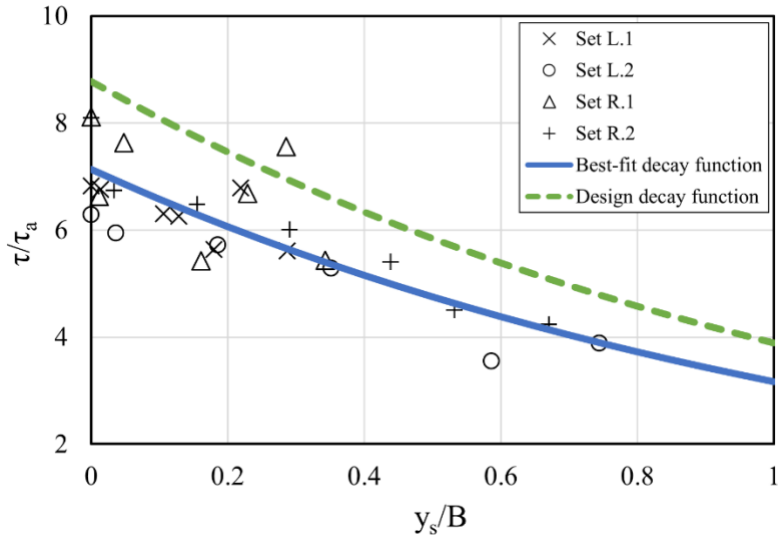

Source: FHWA.

Figure 23. Graph. Decay function for MDOT sets L and R.

Figure 23 indicates that the data from these four cases generally align, and the best fit and the more conservative design decay functions are given in equations 4 and 5, respectively. Shan et al. (2016) used a reliability index (RI) to measure the reliability and accuracy of an equation. The same RI analysis was performed here to make sure the design decay function had an RI of 2.0. To reach that threshold, the best-fit equation was multiplied by a safety factor of 1.23, which resulted in equation 5.

$$\frac{\tau}{\tau_a} = 7.14exp(-0.81\ \frac{y_s}{B}) \quad (4)$$

$$\frac{\tau}{\tau_a} = 8.78ep(-0.81\ \frac{y_s}{B}) \quad (5)$$

CHAPTER 6. TASK 4. CFD SCOUR

A preliminary NextScour CFD scour simulation tool was developed by researchers at FHWA using OpenFOAM, which is open-sourced CFD software (OpenFOAM Foundation Ltd. 2022). A scour model for the simulation tool was written in Python (Python Software Foundation 2022). OpenFOAM was used to simulate the flow condition near the bridge, and the scour model updated the scour bathymetry based on the flow condition output at a given time. The time step for flow simulation varied from 1 to 10 ms, while the scour model ranged from 1 to 30 min. First, the original riverbed information was imported into OpenFOAM as a solid boundary. After one time step of flow calculation, shear stress on the riverbed was extracted and exported to the scour model. The bed surface was deformed to reflect the changing scour depths using the erosion functions for the clay layer (equation 1). The maximum scour depth for one cell in the bed surface was limited to 10 mm per time step. OpenFOAM then resumed the flow simulation with the updated river bathymetry. This iteration between OpenFOAM and the scour model continued until the shear stress in the scour hole equaled the estimated critical shear stress of the soil, i.e., the condition where no further erosion happened.

The average approach bed shear stress in the full-scaled Saginaw River CFD simulation is about 2.7 Pa (0.057 psf) for Q_{100} flow and 3.6 Pa (0.076 psf) for Q_{500} flow. These shear stresses are larger than the critical shear stress of the riverbed sand with a D_{50} of 0.1 mm (0.0039 inch). Therefore, live-bed scour would occur. However, because the current CFD scour tool does not have a sediment transport module, live-bed conditions cannot be simulated. Instead, the critical velocity of the 0.1 mm (0.0039 inch) sand was calculated using the flow depth from Q_{100}. An approach velocity of 0.4 m/s (1.3 ft/s) was used in OpenFOAM simulation, which generated a clear-water flow condition. Due to the shear amplification of the bridge, the flow still eroded sands near the pier and the fender. Once the scour around the bridge pier reached equilibrium, the clay layer at 530 ft was reinserted into the model to generate a new bathymetry, and the bed material properties were updated from 0.1 mm (0.0039 inch) sand to the clay properties measured in Task 2 (figure 24).

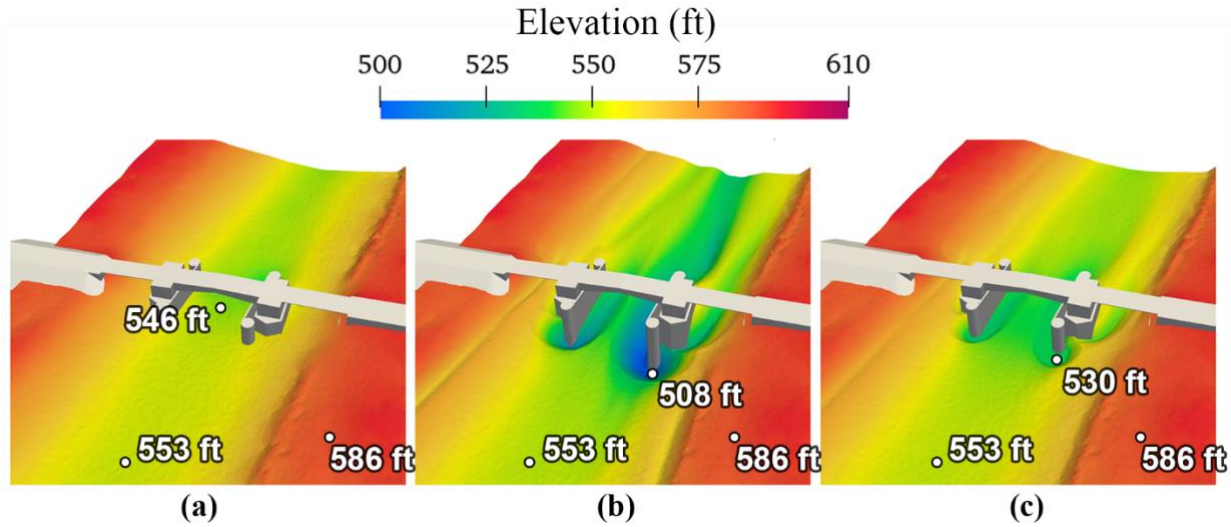

Source: FHWA.

Figure 24. Image. The (a) surveyed riverbed, (b) clear-water scoured riverbed with sand, and (c) the riverbed with clay layer inserted at 530 ft.

Figure 25 illustrates the bed shear stress distributions in the updated bathymetry with the exposed clay layer, and table 4 gives the nominal shear stress magnitudes. Note that the average shear stress value of the left pier consisted of only the exposed clay area, while the average shear stress value of the right pier was bounded by the size of the blockage area. All shear stresses surrounding the two piers under both the Q_{100} and Q_{500} flows were smaller than the critical shear stress of the clay, which was 20.5 Pa (0.431 psf). This result confirmed that scour would stop once the clay layer was exposed. As an exercise, the researchers continuously increased the Q_{500} flow velocity by 10 to 35 percent in increments of 5 while keeping the same WSE to see when flow would start to erode the clay and how much it would erode over time.

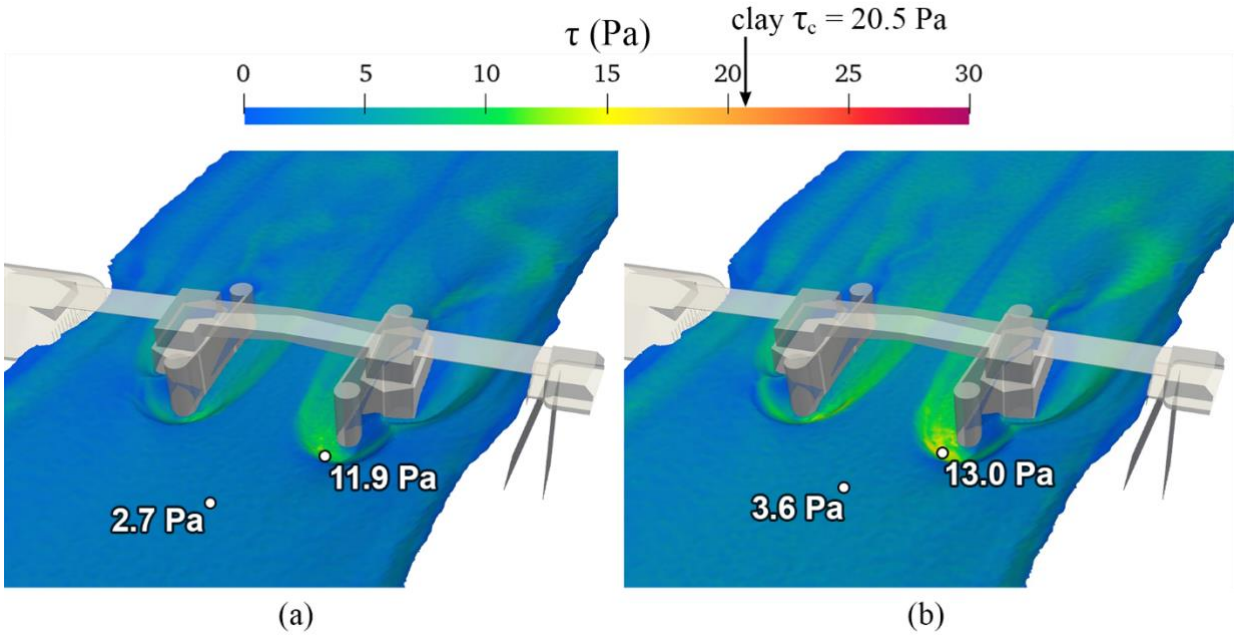

Source: Argonne National Laboratory (ANL). Modifications by FHWA.

Figure 25. Image. Bed shear stress distributions on scoured riverbed with clay layer for (a) Q_{100} discharge and (b) Q_{500} discharge.

The shear stress distributions under the increased flows (figure 26) indicated that bed shear stress started to exceed the clay critical shear stress when the flow reached Q_{500}+30 percent. Under the flow condition of Q_{500}+35 percent, the scour depth in the clay reached 5 ft in a 75-yr simulation near the right upstream fender cylinder (figure 27).

Table 4. Flow conditions and representative shear stresses for increasing flows.

Flow	Flow Rate (cfs)	WSE (ft)	Average Velocity (ft/s)	Clay Exposed Area at Left Pier (ft^2)	Average Shear Stress at Left Pier (Pa)	Flow Blockage Area at Right Pier (ft^2)	Average Shear Stress at Right Pier (Pa)
Q_{100}	59,360	581.3	5.9	523.1	6.5	890.6	10.1
Q_{500}	70,130	582	6.8	525.6	8.7	892.6	12.9
Q_{500}+10%	77,143	582	7.48	525.6	10.7	893.4	15.9
Q_{500}+15%	80,650	582	7.82	525.6	11.8	892.0	17.6
Q_{500}+20%	84,156	582	8.16	525.6	12.9	890.3	19.2
Q_{500}+25%	87,663	582	8.5	525.6	13.9	893.0	20.8
Q_{500}+30%	91,169	582	8.84	525.6	15.0	893.0	22.4
Q_{500}+35%	94,676	582	9.18	525.6	16.2	893.0	24.2

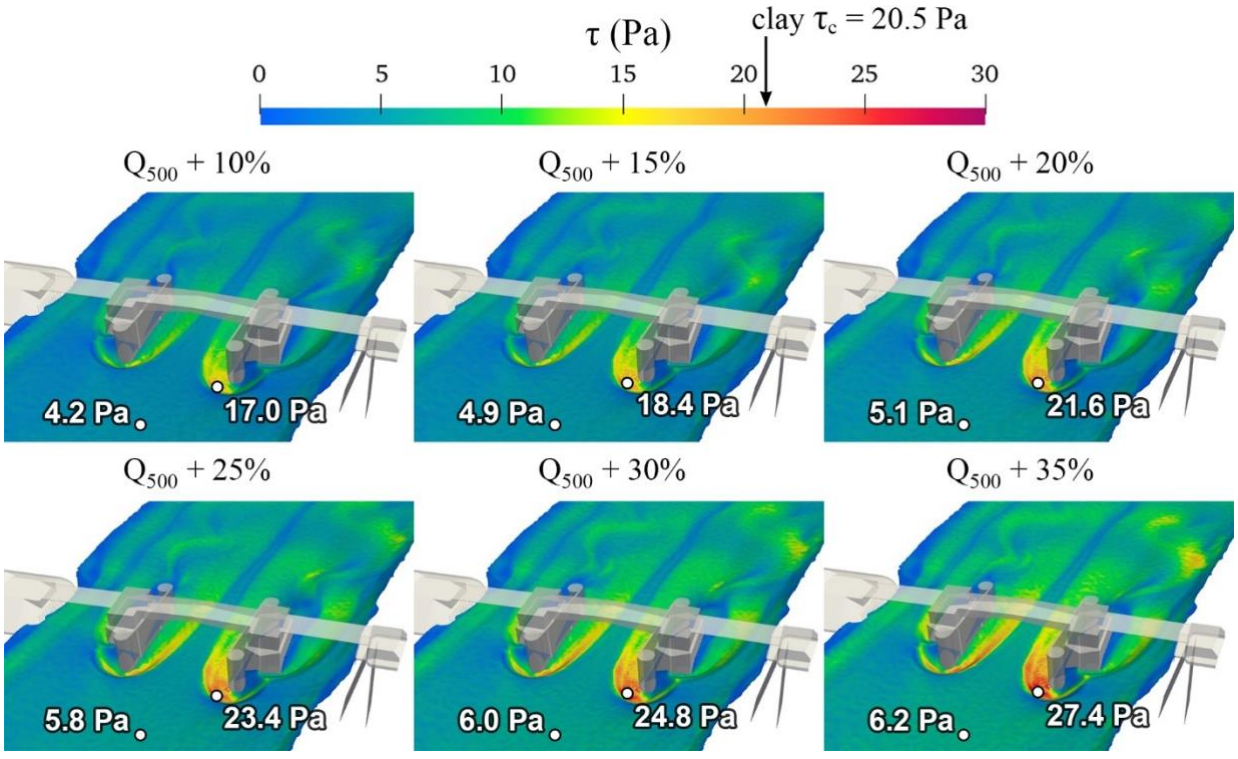

Source: ANL. Modifications by FHWA.

Figure 26. Image. Bed shear stress distributions under increasing flows.

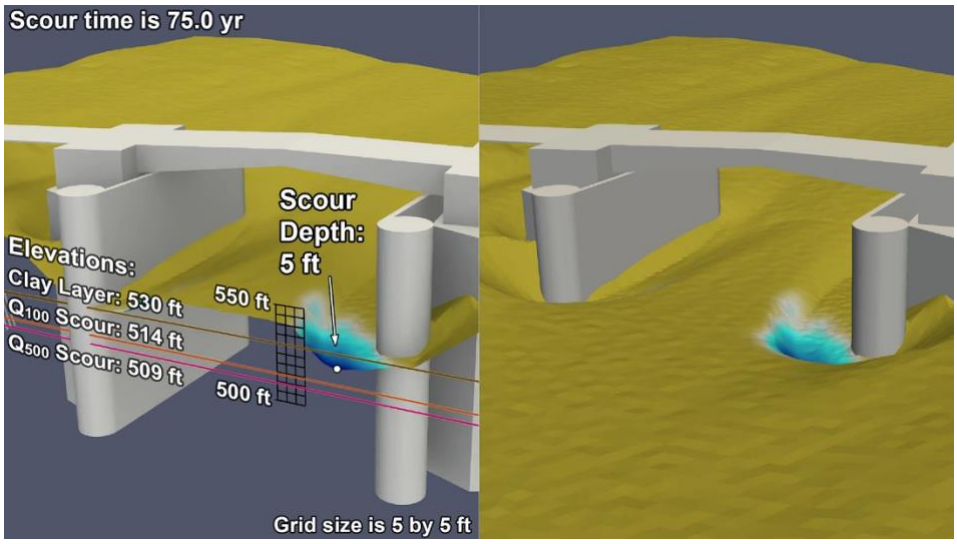

Source: ANL. Modifications by FHWA.

Figure 27. Image. Clay scour depth of 5 ft after Q_{500}+35 percent for 75 yr.

CHAPTER 7. TASK 5. PROBABILISTIC SCOUR ANALYSIS

DETERMINISTIC SCOUR ANALYSIS

The deterministic scour analysis was conducted once the decay function and critical shear stress of the clay layer were known. The design decay function (equation 5) should be used to check whether the clay layer would erode under a given flow.

First, the upstream approach shear stresses, τ_a, for Q_{100} and Q_{500} were computed using equation 6 (equation 6.7 in HEC-18) with given HEC-RAS flow parameters at the approach cross section of station 90 (Arneson et al. 2012).

$$\tau_a = \gamma y^{-\frac{1}{8}} \left(\frac{nV}{K_u}\right)^2 \quad (6)$$

Where:

γ = unit weight of water.
y = approach flow depth.
n = Manning n.
V = average approach velocity.
K_u = 1.486 for English Units and 1.0 for SI Units.

This calculation resulted in approach shear stress values of 11.6 Pa (0.244 psf) and 14.9 Pa (0.313 psf) for the Q_{100} and Q_{500} flows, respectively. The calculated approach shear stress was then converted to bed shear stress at the fender using the ratio from the design equation from equation 5. It should be noted that the approach shear stresses calculated from equation 6 generally overestimate the shear stress compared to the results from CFD simulations because it is averaged over the entire cross section and relies heavily on the estimation of Manning's n value. Alternatively, the CFD calculation considers the velocity profile of the flow and computes the shear stress in the boundary layer of the surface. The values of 11.6 and 14.9 Pa (0.244 and 0.313 psf) were about 4 to 4.5 times greater than the approach shear stress calculated using CFD.

The CFD simulation can more accurately capture the 3D flow pattern near the fender and the bridge piers compared to equation 6. Additionally, because CFD modeling of bed shear stresses at the fender and the piers already considered the contraction effect, no separate contraction scour analysis was needed. Therefore, the initial bed shear stresses calculated near the fender on the riverbed in Task 1 were used as the initial starting condition for the deterministic analysis. These values, originally listed in Table 1, were 14.5 Pa (0.305 psf) for the Q_{100} and 20.2 Pa (0.424 psf) for the Q_{500} flood event. These values were then multiplied by the safety factor of 1.23 used to get the design decay function (equation 5) from the best fit decay function (equation 4). This factor increased the initial bed shear stresses at the pier to 17.8 and 24.8 Pa (0.374 and 0.521 psf). FHWA recognizes that CFD simulations will not be available for all bridge designers, so future research will focus on determining a table of shear stress modification factors to get appropriate initial bed shear stress values at the piers from the approach shear stress calculated in equation 6.

With initial bed shear stress values selected, the decayed shear stress was computed at 1-ft incremental scour depths using equation 5. These shear stresses were compared with clay critical shear stress in the clay layer. Figure 28 reveals that at 530-ft elevation, the decayed shear stress was 13.0 Pa (0.273 psf) for Q_{500}, less than the design clay erosion resistance, which was equal to the mean shear stress minus one standard deviation. Therefore, the total pier scour would stop at 530 ft. This result confirmed the CFD scour results in Task 4.

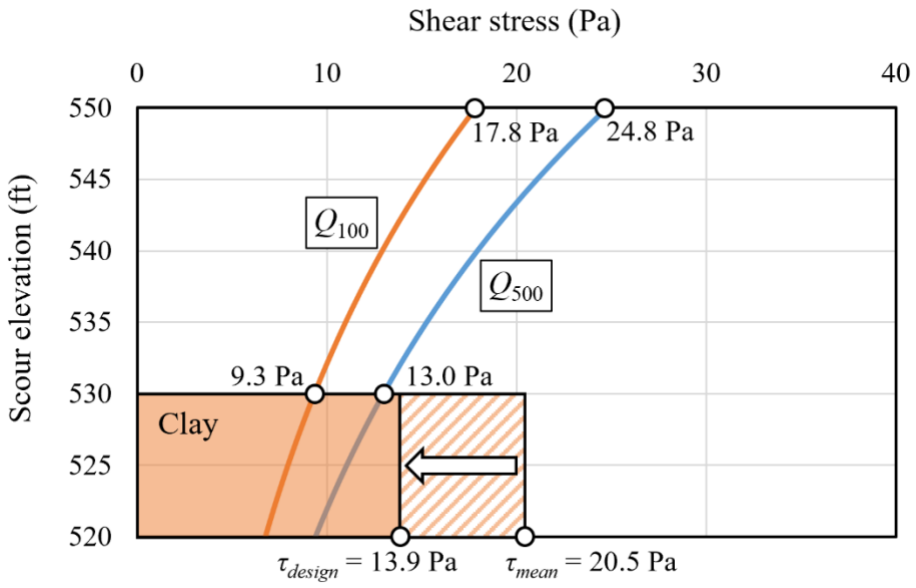

Source: FHWA.
τ_{design} for the clay layer = τ_{mean} − 1 standard deviation (6.6 Pa).

Figure 28. Graph. Deterministic scour analysis using decay function and clay resistance for Q_{100} and Q_{500}.

PROBABILISTIC SCOUR ANALYSIS CONCEPT

In the current American Association of State and Highway Transportation Officials (AASHTO) Load Factor Resistance Design (LRFD) bridge design specifications (2020), the load and resistance generally refer to the forces applied on a bridge structure by internal or external sources and the capability of the designed structure to resist such forces. A typical design limit state equation is as follows:

$$\sum \eta_i \gamma_i L_i \leq \phi R_n \quad (7)$$

Where:

η_i = load modifier.
γ_i = load factor.
L_i = load effect.
ϕ = resistance factor.
R_n = nominal resistance.

Scour is analogous to LRFD, where the load refers to the bed shear stress produced by the flow, and the resistance is the critical shear stress of the soil. When the flow-induced bed shear stress is larger than the critical shear stress of the soil, scour happens. Probability of exceedance, $P_{e,scour}$, represents the probability of the scour going beyond a predicted scour depth. Figure 29(a) shows the concept of load (L) and resistance (R) distribution and $P_{e,scour}$ for a preset scour depth. The distribution of the load, τ_w, is calculated from a Monte Carlo simulation considering various uncertainties in the flood event. The distribution of the resistance τ_c, is obtained from soil erosion tests. The shaded area where the difference between the resistance and load (R - L) is $P_{e,scour}$. A relationship between $P_{e,scour}$ and incremental scour depths can be established, as shown in figure 29(b).

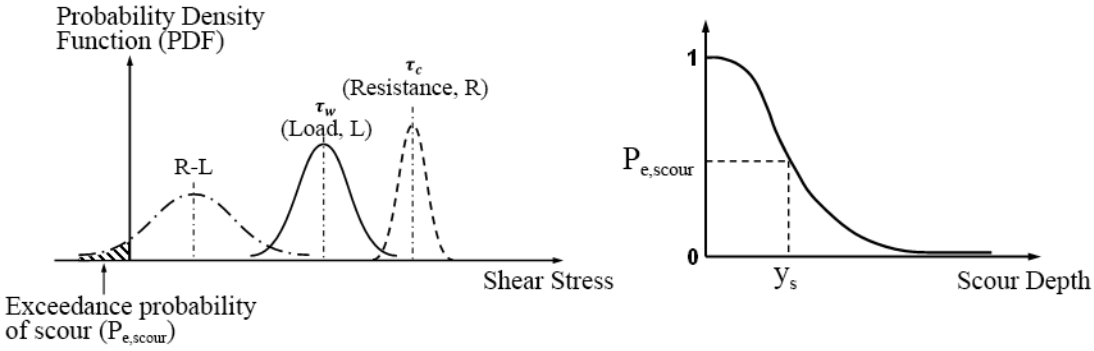

Source: FHWA.

Figure 29. Graph. (a) Load distribution, resistance distribution, and exceedance probability of scour. (b) Exceedance probability versus scour depth.

The probabilistic scour analysis was performed on the proposed new bridge using a 10,000-point Monte Carlo simulation for a 75-yr bridge design life (Doucet et al. 2001). The HEC-RAS model for this project was provided by MDOT. It was a three-reach model with five discharge control cross sections. The HEC-RAS model was revised to a one-reach model with one inlet upstream of the east channel to simplify the probabilistic study.

Step 1: Generate annual maximum discharge.

The U.S. Geological Survey (USGS) gage 04157005 is about 12.5 miles upstream of the Lafayette Avenue Bridge, which does not represent the discharge at the bridge. Therefore, the sample mean ($\bar{X}$), the sample standard deviation (S), and the sample skewness (G) for Log-Pearson Type III distribution were calculated using the peak floods provided in the HEC-RAS model (table 5), and the results were shown in table 6 (Beard 1962; England et al. 2019). The R^2 value for the regression curves was 1.0, which indicated the regression was

accurate. The regressed parameters were used to generate the population mean μ, population standard deviation σ, and population skewness γ. N is the number of the annual peak discharges of the historical record, which was required when determining the distribution of μ, σ, and γ, and S_G. In this case, N was assumed to be 101, the total available annual peak discharges recorded at gage 04157005.

Table 5. Peak-flood statistics at station 140 from HEC-RAS model.

Flow	Q_{10}	Q_{50}	Q_{100}	Q_{500}
Discharge (cfs)	42,785	54,510	59,360	70,130

Table 6. Regressed sample parameters for Log-Pearson Type III distribution.

Parameters	$\bar{X}$	S	G
Station 140	4.446	0.146	-0.112

For 10,000 points Monte Carlo simulation, 10,000 sets of μ_i, σ_i, γ_i (i = 1, 2, … 10,000) were generated. For each set of μ_i, σ_i, γ_i, 75 exceedance probabilities ($P_{e,(i,j)}$, j = 1, 2, … 75) were randomly selected to represent each year of the 75 yr of bridge design life. In total, 750,000 discharges were generated. Figure 30 shows the probability mass function (PMF) of the 750,000 annual maximum discharge and the PMF of the 10,000 maximum annual discharge in every 75 yr at the inlet (station 140).

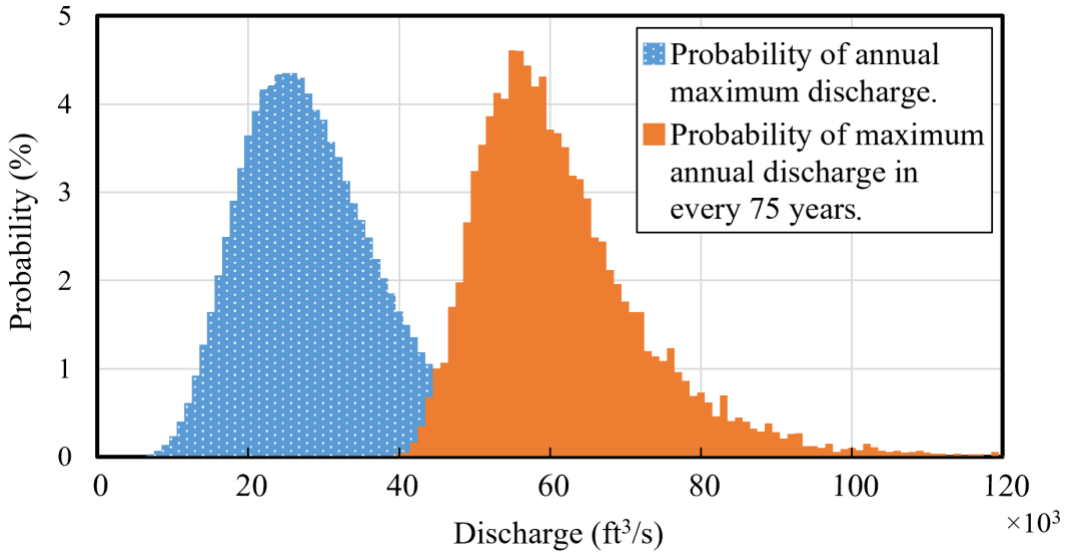

Source: FHWA.

Figure 30. Graph. PMF of annual maximum discharge and maximum annual discharge in every 75 yr for the Lafayette Avenue Bridge (station 140).

The exceedance probability of various flood frequencies calculated from the generated data and the theoretical values were compared in table 7. Generally, the exceedance probability of generated floods in one year was close to the theoretical values. Similarly, the exceedance

probability for 75 yr was also close to the theoretical value for generated floods of Q_{50} and Q_{100}. In contrast, the generated floods of Q_{200} and Q_{500} had a larger exceedance probability in 75 yr than their theoretical values. This result was due to the small number of N used in discharge generation. If N was larger, e.g., N = 1,000 or higher, the Monte Carlo simulation results and the theoretical value would be closer.

Table 7. Comparison of the exceedance probability: Theoretical versus Monte Carlo.

Flood	Exceedance Probability of Flood Frequency in 1 yr		Exceedance Probability of Flood Frequency in 75 yr	
	Theoretical Value (percent)	Monte Carlo (percent)	Theoretical Value (percent)	Monte Carlo (percent)
Q_{50}	2	2.2	78	73.3
Q_{100}	1	1.2	52.9	52.3
Q_{200}	0.5	0.7	31.3	35.2
Q_{500}	0.2	0.3	13.9	19.9

Step 2: Generate Manning's n.

Manning's n is the only random variable considered in the hydraulic model uncertainty, and it is considered constant in the bridge design life. The Transportation Research Board's National Cooperative Highway Research Program (NCHRP) Report 761 indicates that Manning's n follows a lognormal distribution with a COV of 0.015 (Lagasse et al. 2013). Manning's n was given by MDOT as 0.03 for the main channel and 0.08 for the overbanks in the revised HEC-RAS model.

Step 3: Compute the flow conditions in HEC-RAS.

There were 750,000 sets of discharges, and 10,000 Manning's n were submitted to the revised HEC-RAS model via a batch job to compute the flow velocity (V) and flow depth (y_0) at the approach cross section (station 90).

Step 4: Select the scour elevations.

The selected scour elevations were 550, 540, 530, 520, and 510 ft for the total pier scour.

Step 5: Determine the load distribution: Distribution of bed shear stress.

For each scour elevation, 750,000 sets (10,000 sets for each 75-yr bridge design life) of bed shear stresses for the total pier scour ($\tau_{b,total}$) were calculated by using the flow parameters obtained from HEC-RAS (equation 6) and the decay function (equation 4). The load distribution was the distribution of the 10,000 maximum bed shear stresses. Figure 31 shows the probability density function (PDF) of the bed shear stresses at selected scour elevations.

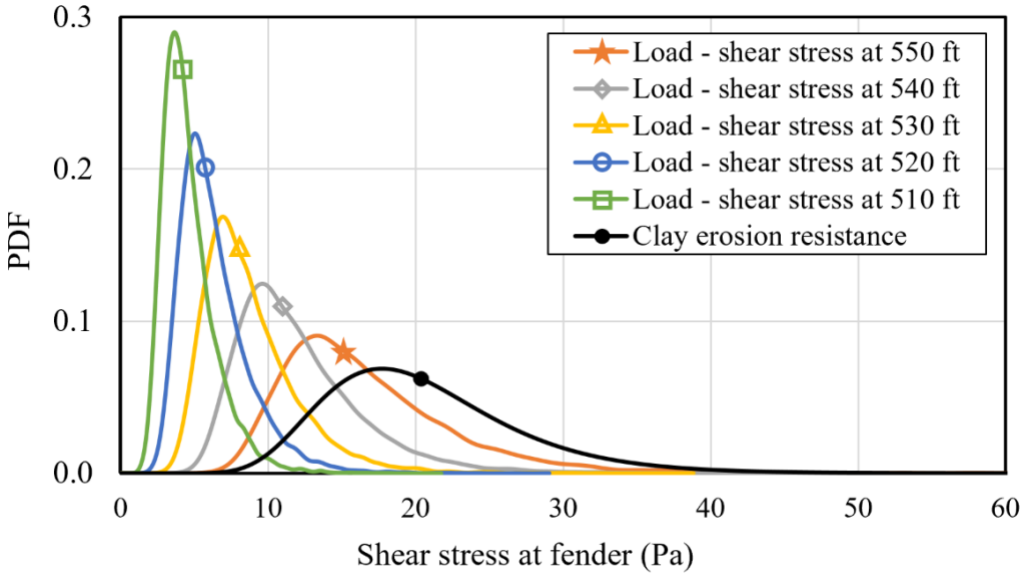

Source: FHWA.

Figure 31. Graph. Bed shear stress distribution for total pier (fender) scour.

Step 6: Distribution of critical shear stress.

It was assumed that the critical shear stress followed a lognormal distribution, whose parameters were calculated from the mean and COV of critical shear stress obtained in Task 2. In that task, 10,000 critical shear stresses were generated according to the obtained lognormal distribution. The "clay erosion resistance" curve in figure 31 shows the PDF of the generated critical shear stresses.

Step 7: Calculate $P_{e,scour}$ at scour elevations.

The load distribution of total pier scour was compared against the resistance distribution. $P_{e,scour}$ was calculated as the probability of critical shear stress being less than the decayed bed shear stress at each target scour elevation. $P_{e,scour}$ at each target scour depth are listed in table 8, as well as shown in figure 32.

Table 8. $P_{e,scour}$ of total pier scour at each scour elevation.

Scour Elevation (ft)	$P_{e,scour}$ for Total Pier Scour (percent)
550	31.6
540	11.5
530	3.3
520	0.7
510	0.2

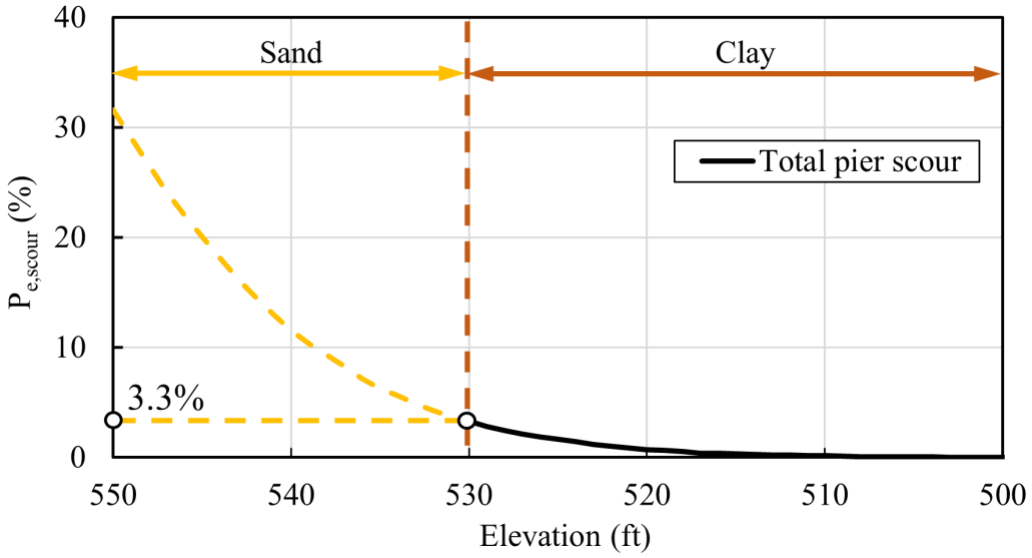

Source: FHWA.

Figure 32. Graph. Exceedance probability for total pier scour at various scour elevations.

PROBABILISTIC SCOUR ANALYSIS BY USING HEC-18 EQUATIONS

A probabilistic scour analysis based on the scour design equations in HEC-18 was performed to identify the exceedance probability of scour depths and compare results with the proposed NextScour decay function method.

For direct comparison, the same distribution on discharge and Manning's *n* and the flow conditions calculated from the HEC-RAS models that were used in the previous probabilistic analysis were adopted here to calculate the exceedance probability for the HEC-18 equations.

For contraction scour, critical velocity, which is calculated by equation 8, was used to determine whether clear water or live-bed condition would apply.

$$V_c = K_u y^{1/6} D_{50}^{1/3} \quad (8)$$

Where:

V_c = critical velocity above which bed material of size D_{50} and smaller will be transported.
y = average depth of flow upstream of the bridge.
D_{50} = particle size in a mixture of which 50 percent are smaller.
K_u = 11.17 for English units or 6.19 for SI units.

According to HEC-18, if the critical velocity of the bed material V_c is larger than the mean velocity upstream of the bridge, the clear water contraction scour equation (equation 9) was used to calculate the contraction scour. Otherwise, the live-bed contraction scour equations (equation 10), were applied.

$$y_{s,contr} = \left\{ \left[\frac{K_u \cdot Q^2}{(1.25 D_{50})^{2/3} \cdot W^2} \right]^{3/7} - y_0 \right\} \cdot f_{Eq,contr} \quad (9)$$

Where:

$y_{s,contr}$ = contraction scour depth.
y_0 = existing depth in the contracted section before scour.
Q = discharge through the bridge associated with the width W.
W = bottom width of the contracted section less pier widths.
K_u = 0.0077 for English units and 0.025 for SI units.
$f_{Eq,contr}$ = equation uncertainty factor for contraction scour.

$$y_{s,contr} = \left[\left(\frac{Q_2}{Q_1}\right)^{6/7} \left(\frac{W_1}{W_2}\right)^{k_1} \cdot y_1 - y_0 \right] \cdot f_{Eq,contr} \quad (10)$$

Where:

y_1 = average depth in the upstream main channel.
Q_1 = flow in the upstream channel.
Q_2 = flow in the contracted channel.
W_1 = bottom width of the upstream main channel.
W_2 = bottom width of main channel in contracted section less pier width.
k_1 = 0.69 for this project.

$f_{Eq,contr}$ in equations 9 and 10 is a factor to account for the equation uncertainty of the contraction scour equations. According to NCHRP Report 761, f_{Eq} follows a normal distribution with the mean and COV of 0.92 and 0.21, respectively (Lagasse et al. 2013).

The local pier scour depth was calculated using equation 11:

$$y_{s,pier} = \left[2 \cdot K_1 \cdot K_2 \cdot K_3 \cdot \left(\frac{a}{y_1}\right)^{0.65} \cdot Fr^{0.43} \cdot y_1 \cdot K_w \right] \cdot f_{Eq,pier} \quad (11)$$

Where:

$y_{s,pier}$ = local pier scour depth.
y_1 = flow depth directly upstream of the pier.
K_1 = correction factor for pier nose shape (K_1 = 1.0 for this project).
K_2 = correction factor for angle of attack of flow (K_2 = 1.2 for this project).
K_3 = correction factor for bed condition (K_3 = 1.1 for this project).
a = pier width (a = 53.75 ft for this project).
Fr = Froude number.
K_w = correction factor for wide piers.
$f_{Eq,pier}$ = equation uncertainty factor for pier scour.

Fr is calculated using equation 12:

$$Fr = \frac{V}{\sqrt{g \cdot y_1}} \tag{12}$$

Where:

V = flow velocity directly upstream of the pier.
y_1 = flow depth directly upstream of the pier.
g = gravitational constant.

K_w, the correction factor for wide piers, is calculated by equation 13 for clear-water conditions and equation 14 for live-bed conditions, respectively.

$$K_w = 2.58 \cdot \left(\frac{y_1}{a}\right)^{0.34} \cdot Fr^{0.65} \tag{13}$$

$$K_w = 1.0 \cdot \left(\frac{y_1}{a}\right)^{0.13} \cdot Fr^{0.25} \tag{14}$$

$f_{Eq,pier}$ in equation 11 is a factor to account for the equation uncertainty of the local pier scour equation. According to NCHRP Report 761, $f_{Eq,pier}$ follows a normal distribution with the mean and COV of 0.82 and 0.23, respectively (Lagasse et al. 2013).

The total pier scour ($y_{s,total}$) was the sum of the contraction scour and local pier scour depth, as shown in equation 15:

$$y_{s,total} = y_{s,contr} + y_{s,pier} \tag{15}$$

A total of 750,000 contraction ($y_{s,contr}$), local pier ($y_{s,pier}$), and total pier scour depths ($y_{s,total}$) were calculated from 750,000 flow conditions obtained at Step 3 in the previous section by using equations 9 or 10, equation 11, and equation 15. For every 75-yr bridge life, 10,000 maximum contraction ($y_{s,contr,max}$), local pier ($y_{s,pier,max}$), and total pier scour depth ($y_{s,total,max}$) values were obtained. The exceedance probability of scour depth was computed by 1 minus the empirical cumulative distribution function of the 10,000 maximum scour depth for each scour component, and the results are shown in figure 33 through figure 35.

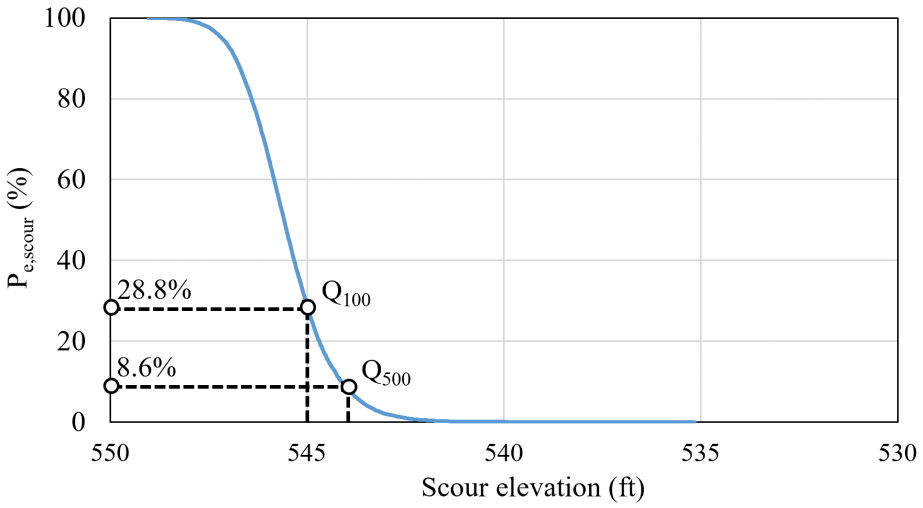

Source: FHWA.

Figure 33. Graph. Exceedance probability of contraction scour at various scour elevations.

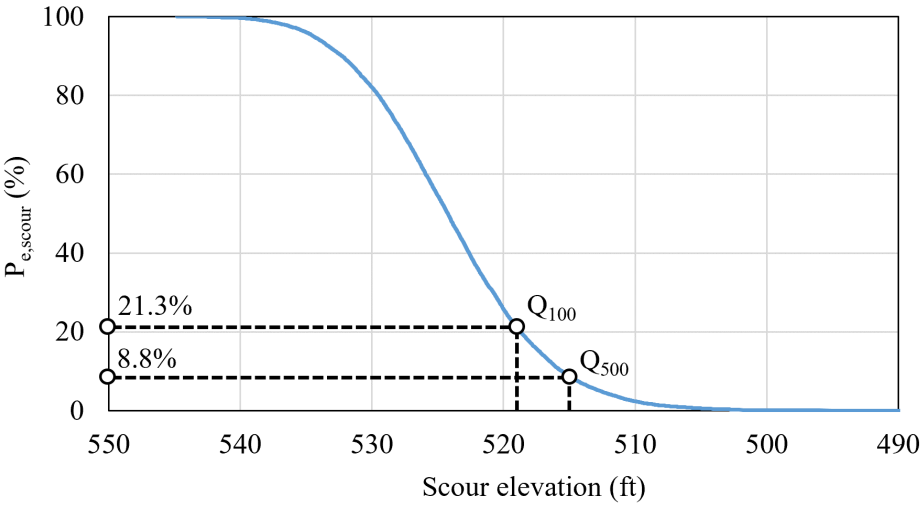

Source: FHWA.

Figure 34. Graph. Exceedance probability of local pier scour at various scour elevations.

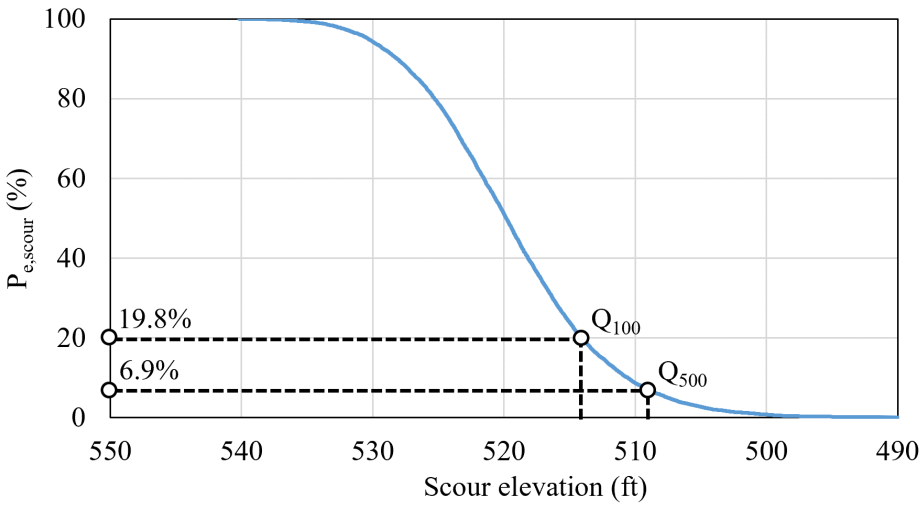

Source: FHWA.

Figure 35. Graph. Exceedance probability of total pier scour at various scour elevations.

A summary of the original MDOT scour analysis is shown in table 9. It was observed that the exceedance probability of the design contraction scour depth for Q_{100} and Q_{500} flood is 28.8 and 8.6 percent, respectively; the exceedance probability of the design local pier scour depth for Q_{100} and Q_{500} flood is 21.3 and 8.8 percent, respectively; and the exceedance probability of the design total pier scour depth for Q_{100} and Q_{500} flood is 19.8 and 6.9 percent, respectively.

Table 9. Design scour depth for Q_{100} and Q_{500} flood.

Scour Component	Q_{100}			Q_{500}		
	Scour Depth (ft)	Elevation (ft)	Exceedance Probability (percent)	Scour Depth (ft)	Elevation (ft)	Exceedance Probability (percent)
Contraction scour	5	545	28.8	6	544	8.6
Local pier scour	31	519	21.3	35	515	8.8
Total pier scour	36	514	19.8	41	509	6.9

Figure 36 compares the exceedance probabilities calculated by using the NextScour decay function method and HEC-18 equations. The deterministic analysis with the NextScour decay function method shows that the scour elevation for Q_{100} and Q_{500} flood can be increased from 514 ft and 509 ft (determined by HEC-18 equation) to 530 ft (determined by decay function). With the probabilistic analysis, the exceedance probabilities of the total pier scour depth for Q_{100} and Q_{500} flood can be reduced from 19.8 and 6.9 percent to 3.3 percent. The significant improvement mainly attributes to the consideration of soil erosion resistance at the clay layer when using the decay function. It was found that the proposed decay function method was able to achieve a shallower scour depth with less uncertainty compared to the scour design by using the existing HEC-18 equations, which assume a uniform sand layer.

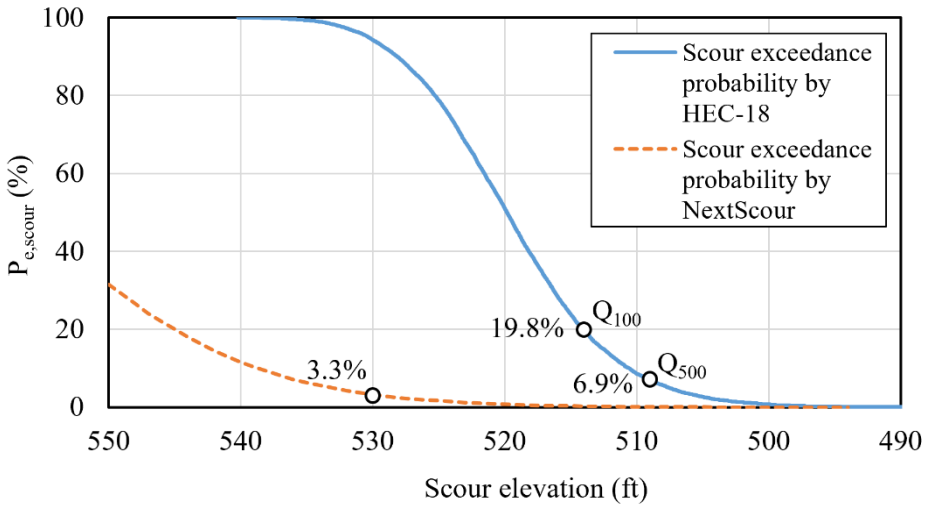

Source: FHWA.

Figure 36. Graph. Comparison of exceedance probability of total pier scour.

CHAPTER 8. SUMMARY

The Lafayette Avenue Bridge replacement project provided an excellent candidate for the TPF study. CFD modeling, physical flume scour testing, and soil erosion testing were all conducted by researchers in the FHWA Hydraulics Laboratory.

Hydraulic modeling using 2D and 3D models found an initial representative CFD shear stress of 14.5 Pa (0.305 psf) for Q_{100} and 20.2 Pa (0.424 psf) for Q_{500} at the riverbed near the left upstream fender cylinder. Physical modeling included fabricating two 1:50 scale half-bridge models for flume scour tests. Various approach velocities were used to observe the scour around fender cylinders, piers, and abutments. Scour tests revealed that the deepest scour happened upstream of the fender cylinders, and abutment scour was minimal.

CFD-computed bed shear stresses on incremental scour bathymetries, which were collected from the flume scour tests, were used to develop the decay functions of scour at the fenders. Soil erosion tests identified that the clay below the 530-ft elevation had a mean critical shear stress of 20.5 Pa (0.431 psf) with a COV of 0.32.

A probabilistic scour analysis approach was considered using the Monte Carlo simulation. Nearly a million flow discharges were generated using a batch HEC-RAS computation that considered various statistical uncertainties in the flood event and a distribution of Manning's *n* values. With the decay function equations and the computed approach shear stresses from the resulting Monte Carlo flow parameters, the distribution of decayed shear stress at 1-ft incremental scour depth was calculated. The exceedance probability of the total fender scour for a continuous depth was determined by comparing the decayed shear stress against the soil resistance distribution at each depth. The exceedance probability of the total fender scour reaching the clay layer at 530 ft was determined to be 3.3 percent in the 75-yr bridge design life. For comparison, the probabilistic scour analysis was also performed by using the HEC-18 equation, in which the exceedance probability of the design total fender scour depth was 19.8 and 6.9 percent for Q_{100} and Q_{500} flood, respectively. It was found that by using the decay function, which considered the resistance of the clay layer, the exceedance probability of total fender scour depth for Q_{100} and Q_{500} flood reduced from 19.8 and 6.7 percent, respectively, to 3.3 percent.

This study result provides MDOT with a research tool to quantify a risk level in bridge foundation design. It also demonstrated NextScour could significantly improve the accuracy of bridge scour estimates. Future monitoring of the bridge site is recommended, however, to verify the scour predictions after a flood event.

REFERENCES

AASHTO. 2020. *AASHTO LRFD Bridge Design Specifications, 9th Edition*. Report No. LRFDBDS-9. Washington, DC: American Association of State and Highway Transportation Officials.

Arneson, L., L. Zevenbergen, P. Lagasse, and P. Clopper. 2012. *Hydraulic Engineering Circular No. 18, Evaluating Scour at Bridges, Fifth Edition*. Report No. FHWA-HIF-12-003. Washington, DC: Federal Highway Administration.

Beard, L. R. 1962. *Statistical Methods in Hydrology*. Report No. TD-4. Davis, CA: U.S. Army Corps of Engineers, Hydrologic Engineering Center.

Briaud, J. L., H. C. Chen, K. A. Chang, S. J. Oh, S. Chen, J. Wang, Y. Li, K. Kwak, P. Nartjaho, R. Gudaralli, W. Wei, S. Pergu, Y. W. Cao, and F. Ting. 2011. *The Sricos—EFA Method Summary Report*. College Station, TX: Texas A&M University.

Doucet, A., N. Freitas, and N. Gordon. 2001. *Sequential Monte Carlo Methods in Practice*. New York: Springer.

England, J. F., T. A. Cohn, B. A. Faber, J. R. Stedinger, W. O. Thomas, Jr.., A. G. Veilleux, J. E. Kiang, and R. R. Mason, Jr. 2019. *Guidelines for Determining Flood Flow Frequency, Bulletin 17-C*. Reston, VA: U.S. Geological Survey Techniques and Methods, book 4, chap. B5, 148. https://doi.org/10.3133/tm4B5, last accessed October 27, 2022.

Federal Highway Administration. 2020. *Soil and Erosion Testing Services for Bridge Scour Evaluations.* TPF-5(461). Washington, DC: Federal Highway Administration. https://www.pooledfund.org/Details/Study/688, last accessed October 5, 2022.

Lagasse, P. F., M. Ghosn, P. A. Johnson, L. W. Zevenbergen, and P. E. Clopper. 2013. *Reference Guide for Applying Risk and Reliability-Based Approaches for Bridge Scour Prediction*. NCHRP Report 761. Washington, DC: Transportation Research Board.

Moody, L. F. 1944. "Friction factors for pipe flow." *Transactions of the American Society Mechanical Engineers*, 66, no. 8: 671–684.

OpenFOAM Foundation Ltd. 2022. *OpenFOAM* (software). Version 8. https://openfoam.org, last accessed October 21, 2022.

Python Software Foundation. 2022. *Python* (software). Version 3.9.7. https://www.python.org/, last accessed October 21, 2022.

Shan, H., R. Kilgore, J. Shen, and K. Kerenyi. 2016. *Updating HEC-18 Pier Scour Equations for Noncohesive Soils*. Report No. FHWA-HRT-16-045. Washington, DC: Federal Highway Administration. https://www.fhwa.dot.gov/publications/research/infrastructure/structures/bridge/16045/16045.pdf, last accessed October 5, 2022.

Shan, H., A. Wagner, K. Kerenyi, J. Guo, and Z. Xie. 2011. "An Ex-Situ Scour Testing Device for Erosion Research of Cohesive Soils." *Proceedings of the 2011 Engineering Mechanics Institute Conference*. Boston, MA: American Society of Civil Engineers. 1020–1027.

Shan, H., J. Pagenkopf, K. Kerenyi, C. Huang. 2021a. "NextScour for Improving Bridge Scour Design in the United States." *Proceedings of the Institution of Civil Engineers–Forensic Engineering*, 173, no. 4: 121–129. https://doi.org/10.1680/jfoen.20.00017, last accessed October 5, 2022.

Shan, H., O. Wiblishauser, K. Kerenyi, M. Uhrig, C. Huang, and J. Pagenkopf. 2021b. "Efficient Automated Laboratory Testing of Erosion Resistance for Fine-Grained Soils." *Proceedings of the 10th International Conference on Scour and Erosion*. Arlington, VA: American Society of Civil Engineers. 1063–1071.

Stine, R. 1989. "An Introduction to Bootstrap Methods: Examples and Ideas." *Sociological Methods and Research*, 18, nos.2 and 3: 243–291.

USACE. 2022. *Hydrologic Engineering Center's River Analysis System* (*HEC-RAS*) (software). Version 6.3.

U.S. Bureau of Reclamation. 2022. Technical Service Center. Sedimentation and River Hydraulics—Two-Dimension (SRH-2D) (software). Version 2.

Recommended citation: Federal Highway Administration,
NextScour Case Study: The Lafayette Avenue Bridge Over the Saginaw River in Bay City, Michigan
(Washington, DC: 2023) https://doi.org/10.21949/1521957

HRDI-40/01-23(WEB)E